DIABETES

A nanofibrous encapsulation device for safe delivery of insulin-producing cells to treat type 1 diabetes

Xi Wang[1], Kristina G. Maxwell[2,3], Kai Wang[4,5], Daniel T. Bowers[1], James A. Flanders[6], Wanjun Liu[1], Long-Hai Wang[1], Qingsheng Liu[1], Chengyang Liu[7], Ali Naji[7], Yong Wang[8], Bo Wang[1], Jing Chen[1], Alexander U. Ernst[1], Juan M. Melero-Martin[4,5,9], Jeffrey R. Millman[2,3]*, Minglin Ma[1]*

Transplantation of stem cell–derived β (SC-β) cells represents a promising therapy for type 1 diabetes (T1D). However, the delivery, maintenance, and retrieval of these cells remain a challenge. Here, we report the design of a safe and functional device composed of a highly porous, durable nanofibrous skin and an immunoprotective hydrogel core. The device consists of electrospun medical-grade thermoplastic silicone-polycarbonate-urethane and is soft but tough (~15 megapascal at a rupture strain of >2). Tuning the nanofiber size to less than ~500 nanometers prevented cell penetration while maintaining maximum mass transfer and decreased cellular overgrowth on blank (cell-free) devices to as low as a single-cell layer (~3 micrometers thick) when implanted in the peritoneal cavity of mice. We confirmed device safety, indicated as continuous containment of proliferative cells within the device for 5 months. Encapsulating syngeneic, allogeneic, or xenogeneic rodent islets within the device corrected chemically induced diabetes in mice and cells remained functional for up to 200 days. The function of human SC-β cells was supported by the device, and it reversed diabetes within 1 week of implantation in immunodeficient and immunocompetent mice, for up to 120 and 60 days, respectively. We demonstrated the scalability and retrievability of the device in dogs and observed viable human SC-β cells despite xenogeneic immune responses. The nanofibrous device design may therefore provide a translatable solution to the balance between safety and functionality in developing stem cell–based therapies for T1D.

INTRODUCTION

The replacement of inadequate β cells has been proposed as a promising therapy for type 1 diabetes (T1D) (*1*, *2*). Clinical trials with intrahepatic allogeneic islet transplantation have shown insulin independence in patients with diabetes (*3*–*5*), but factors including the instant blood-mediated inflammatory reaction, the side effects of immunosuppressive drugs, and the shortage of human islets from cadavers limit application to patients. Stem cell–derived β (SC-β) cells could provide a nearly unlimited supply of cells and therefore holds great promise for treating T1D (*6*–*11*). However, the potential risks of immunosuppression and teratoma formation by undifferentiated stem cells remain formidable concerns (*12*–*14*). Therefore, the delivery of SC-β cells in a retrievable, immunoprotective encapsulation device that is both safe (prevents any potential cell escape) and functional (maintains facile mass transfer) may be critical to the clinical success of stem cell–based therapies for T1D.

Alginate microcapsule–based encapsulation systems have been extensively investigated and proven functional in multiple animal models (*15*–*21*). However, it is becoming increasingly recognized that the impossibility to ensure complete graft retrieval will hinder their application for SC-β cell delivery in clinical settings. To take advantage of the biocompatibility and immunoprotective property of alginate hydrogels while endowing retrievability, our laboratory has recently developed a thread-reinforced alginate fiber for islet encapsulation (TRAFFIC) device (*22*). Similar to alginate microcapsules, TRAFFIC maintained cell viability and reversed diabetes in mouse models. Unlike microcapsules, TRAFFIC was completely retrievable using a laparoscopic procedure. However, alginate and hydrogels are intrinsically weak relative to other materials such as elastomers and prone to swelling and even breakage over time. This increases the risk of exposing transplanted cells to the host immune system and allowing undifferentiated cells to escape from the device.

In comparison, polymer-based encapsulation devices such as those made of semipermeable polytetrafluoroethylene membranes (for example the TheraCyte device or the ViaCyte device) (*23*–*28*) are sturdy and can prevent potential cell escape, representing a safer and more translatable strategy for developing cell replacement therapies. However, their small pore sizes (on the order of ~100 nm) and foreign body reaction (FBR)–induced fibrotic deposition diminish mass transfer that is critical for long-term function. Similarly, a polycaprolactone (PCL) nanoporous membrane formed around sacrificial nanorods was used to form durable encapsulation devices (for example the Encellin device) (*29*, *30*), but the small pore size (on the order of ~10 nm) and biodegradability of PCL makes the long-term, reliable membrane function less certain, posing a risk for clinical applications. In addition, in many of these devices, extra layers of more rigid membranes, such as polyethylene terephthalate mesh, are often required to give mechanical support to the devices and maintain their planar shape in vivo. These additional rigid layers may increase the severity of FBR and negatively affect the function. Last, these devices have been designed for subcutaneous (S.C.) implantation, which is challenging due to the low degree of vasculature and limited oxygen supply in the S.C. space (*31*).

[1]Department of Biological and Environmental Engineering, Cornell University, Ithaca, NY 14853, USA. [2]Division of Endocrinology, Metabolism and Lipid Research, Washington University School of Medicine, St. Louis, MO 63110, USA. [3]Department of Biomedical Engineering, Washington University in St. Louis, St. Louis, MO 63130, USA. [4]Department of Cardiac Surgery, Boston Children's Hospital, Boston, MA 02115, USA. [5]Department of Surgery, Harvard Medical School, Boston, MA 02115, USA. [6]Department of Clinical Sciences, Cornell University, Ithaca, NY 14853, USA. [7]Department of Surgery, Hospital of the University of Pennsylvania, Philadelphia, PA 19104, USA. [8]Division of Transplant Surgery, University of Virginia, Charlottesville, VA 22904, USA. [9]Harvard Stem Cell Institute, Cambridge, MA 02138, USA.
*Corresponding author. Email: mm826@cornell.edu (M.M.); jmillman@wustl.edu (J.R.M.)

Here, we report an intraperitoneal (I.P.), tubular, nanofiber-integrated cell encapsulation (NICE) device that is both safe and functional long term for delivery of insulin-producing cells including human SC-β cells. The device consists of a highly porous and durable nanofibrous skin made by electrospinning a biocompatible medical-grade thermoplastic silicone-polycarbonate-urethane (TSPU) and an alginate hydrogel core, which provides additional immunological protection and maintains the separation of islets or SC-β cells within the device. The device can be implanted and retrieved using laparoscopic procedures. The nanofibrous skin contains interconnected pores of tunable size, and the device pores are on the order of ~1 μm. Live imaging and histological analysis confirmed the continuous containment of encapsulated cells for 5 months; the device restored normoglycemia in diabetic mice for up to 200 days, including when human SC-β cells were used to reverse diabetes in immunodeficient and immunocompetent mice. We also demonstrate the scalability and retrievability of the NICE device with human SC-β cells in dogs. The NICE design may therefore provide a translatable solution to the balance between safety and functionality in developing a stem cell–based cell replacement therapy for T1D.

RESULTS

Design, fabrication, and characterization of the NICE device

We designed the NICE device based on several criteria: mechanical toughness to ensure long-term stability and safety, tubular form for high-surface area and minimally invasive implantation and retrieval, biocompatibility with host tissue (minimal FBR), sufficiently small pores to prevent cell escape but high porosity to ensure facile mass transfer, and low complexity of design to facilitate translation (Fig. 1A). We chose a biocompatible medical-grade TSPU as the polymer and used electrospinning to fabricate the device due to its ability to produce tough, nanofibrous membranes with tunable and interconnected pore structures.

Nanofibers were collected on a rotating, sugar-coated mandrel template (fig. S1A), and nanofibrous tubes were obtained after dissolution of the sugar coating. The tubes had inner diameters ranging from 500 μm to 3 mm and a wall thickness of ~100 μm (Fig. 1A). Examination using a scanning electron microscope verified the nonwoven fibrous nature of the NICE membrane with an average fiber diameter of 270 nm (Fig. 1A). Tensile tests demonstrated that the nanofibrous tube remained elastically deformable up to about 5 MPa under a 0.5 strain. The ultimate tensile strength was about 15 MPa at a device strain greater than 2. The Young's modulus calculated from 10 to 20% of the curve is ~12.6 ± 0.6 MPa (n = 4) (Fig. 1B). Qualitatively, the device can be stretched more than three times its original length (Fig. 1C and movie S1), bent without kinks (Fig. 1D and movie S2), and handled using forceps without damage.

Knowing the mechanical strength of the device, we next investigated the mass transfer properties and compatibility with islets. A static glucose-stimulated insulin secretion (GSIS) test showed that mouse islets encapsulated in the NICE device were capable of responding to low and high glucose, with a mean stimulation index (SI) (insulin secretion at high glucose to that at low glucose) of 2.33 and 4.23 after 1 and 7 days of culture, respectively (Fig. 1E). The SI of islets cultured inside the device was not significantly different from that of freely floating islets after 1 day (2.33 ± 1.23 versus 2.34 ± 0.13) (P = 0.9888) or 7 days (4.23 ± 0.72 versus 3.39 ± 1.44) (P = 0.5794) of culture (Fig. 1E). The live/dead staining and corresponding quantitative analysis indicated similar viability (~95%) of

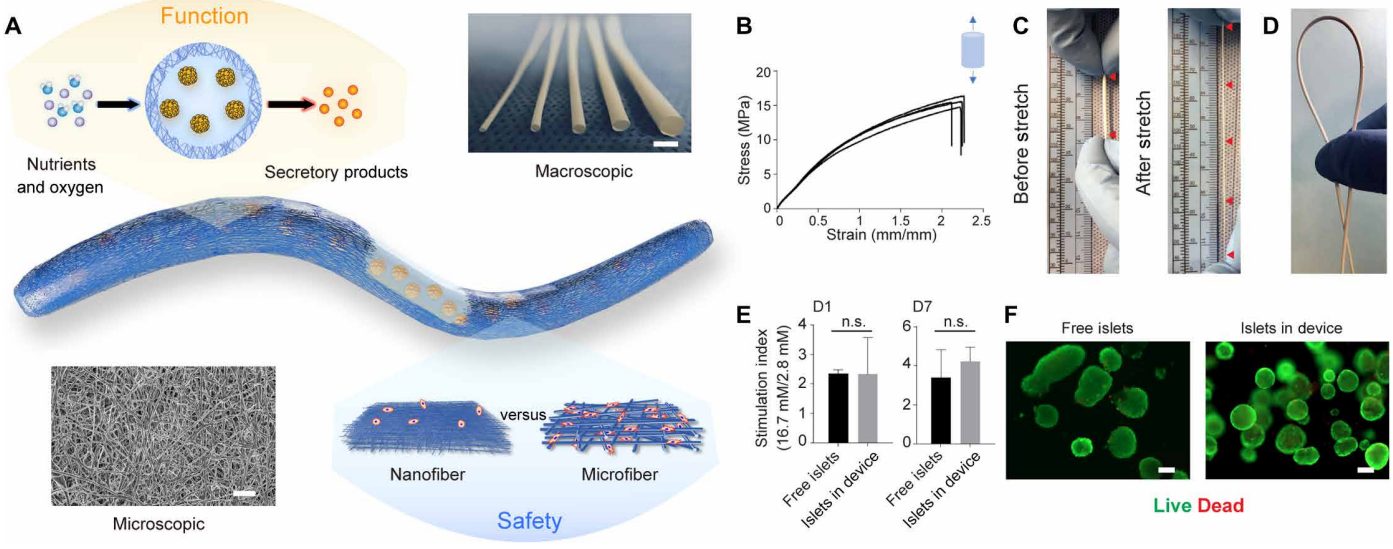

Fig. 1. Design and characterization of the NICE device including mechanical properties, permeability, and cell compatibility. (**A**) Schematics of the device showing the islet-laden hydrogel core surrounded by the nanofibrous skin that prevents cell penetration while allowing maximum mass transfer, along with a photo of nanofibrous tubes with different diameters (from left to right: 0.5, 1, 1.5, 2, and 3 mm) and a scanning electron microscope image of the nanofibers. (**B**) Tensile test (stress-strain curves) of the nanofibrous tubes (n = 4). (**C** and **D**) Photographs showing the device being stretched more than three times in length (C) and bent without kink (D). (**E**) SI of mouse islets (the ratio of insulin secretion in the buffers of high- and low-glucose concentrations) encapsulated in the device, compared to that of free-floating islets after 1 and 7 days of culture; mean ± SD (n = 3). (**F**) Live (green) and dead (red) staining of free-floating islets and islets encapsulated in device after 1-day culture. The data were compared using the two-tailed Student's t test. Scale bars, 3-mm (A) macroscopic image and 100- (F) and 5-μm (A) microscopic images. n.s., nonsignificant.

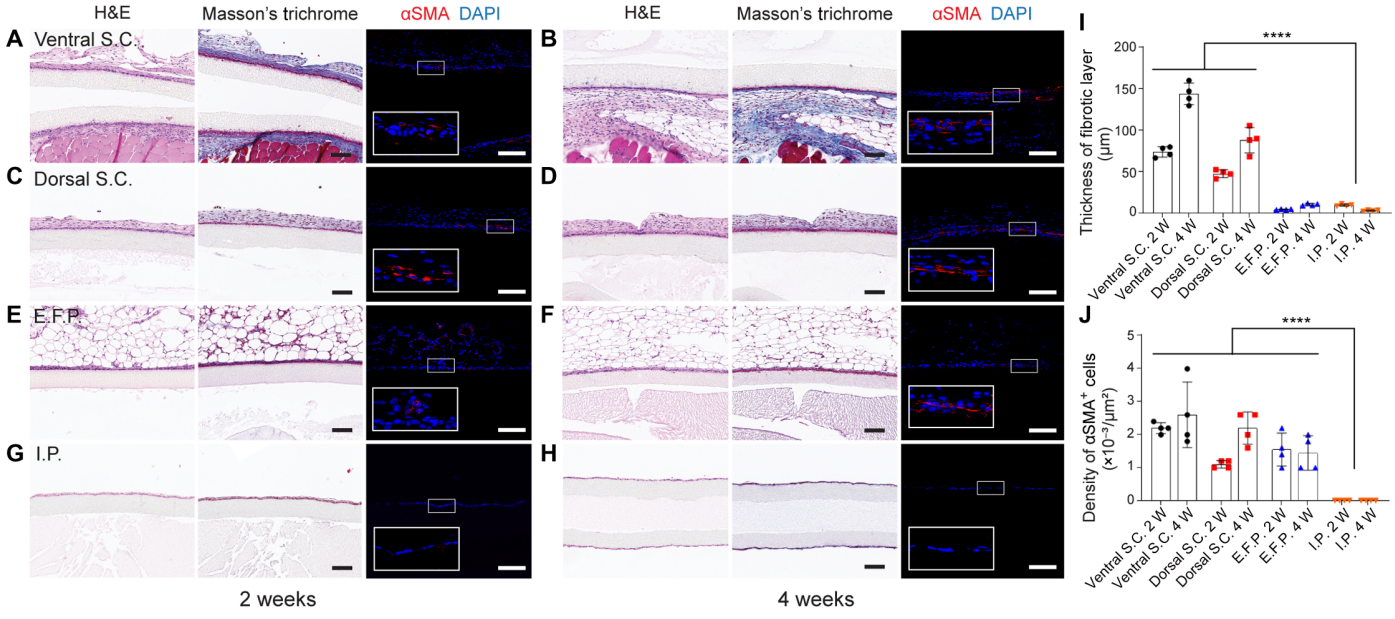

Fig. 2. Biocompatibility of blank (cell-free) devices in different implantation sites in healthy mice for 2 and 4 weeks. (**A** to **H**) Blank (cell-free) devices implanted in the ventral S.C. space for 2 (A) and 4 weeks (B), in the dorsal S.C. space for 2 (C) and 4 weeks (D), in the E.F.P. for 2 (E) and 4 weeks (F), and the in I.P. space for 2 (G) and 4 weeks (H). In each panel, representative images from left to right are H&E staining, Masson's trichrome staining, and immunofluorescent staining. Myofibroblasts were stained with αSMA (shown in red) and DAPI (shown in blue). (**I**) Analysis of the thickness of fibrotic layer measured from Masson's trichrome staining images; mean ± SD ($n = 4$). (**J**) Analysis of the αSMA^+ cells measured from immunofluorescent staining images; mean ± SD ($n = 4$). The data were compared using one-way ANOVA followed by Tukey's test. ****$P < 0.0001$. Scale bars, 100 μm (A to H). S.C., subcutaneous; E.F.P., epididymal fat pad; I.P., intraperitoneal; H&E, hematoxylin and eosin; αSMA, α–smooth muscle actin.

islets inside the device to free islets after 24-hour culture (Fig. 1F and fig. S1B). These in vitro experiments demonstrated that the NICE device met the basic requirements as a cell delivery vehicle, providing sufficient mass transfer and cell compatibility to ensure the function of islets.

Biocompatibility of the NICE device in the I.P. space of mice

The in vivo biocompatibility of an encapsulation device is an important factor; FBR-induced fibrotic deposition can diminish the mass transfer and affect the function of encapsulated cells. We implanted and compared the FBR to the blank (cell-free) NICE devices in three clinically relevant transplant sites: the I.P. space, the epididymal fat pad (E.F.P.) (as a model of the omentum in large mammals), and the S.C. space in C57BL/6 mice. Hematoxylin and eosin (H&E) staining and Masson's trichrome staining demonstrated that the devices implanted in either the ventral or dorsal S.C. space formed a thick fibrotic capsule (more than 40 μm) (Fig. 2, A to D and I). The thickness of the fibrotic layer at the 4-week time point was significantly ($P < 0.0001$) increased compared to that at 2 weeks in both the dorsal S.C. space (87.7 ± 13.2 versus 47.3 ± 4.1 μm) and the ventral S.C. space (143.5 ± 11.3 versus 73.6 ± 5.4 μm) (Fig. 2I). In contrast, devices implanted in the I.P. space or the E.F.P. had much thinner cellular overgrowth (less than ~10 μm) than in the S.C. space (Fig. 2, E to I). Although there was no statistically significant difference between the I.P. space and E.F.P. at either 2 ($P = 0.9754$) or 4 weeks ($P = 0.8610$), the cellular overgrowth on the device in the I.P. space at 4 weeks was only a single layer of cells with thickness of 2.9 ± 0.6 μm. Devices implanted in the E.F.P. or the S.C. space were wrapped tightly within tissue. It was noted that the nanofibrous membranes remained impenetrable to cells in all locations.

Myofibroblasts that are present in fibrotic capsules are identifiable by their expression of α–smooth muscle actin (αSMA). These cells can arise from cell populations that enter the vicinity of a foreign material such as macrophages (*32*) and may be of bone marrow origin (*33*). The number and density of myofibroblasts trended with the fibrotic layer thickness (Fig. 2, I and J). More αSMA^+ cells were observed in the S.C. space than in the I.P. space. There was no expression of αSMA in the I.P. group and no foreign body giant cells were found adjacent to the implant surface. Thus, the FBR was determined to be the least severe in the I.P. space, motivating the choice to investigate this implantation site in this study.

We hypothesized that the low FBR was due to unique properties of TSPU and the small fiber size. To test this hypothesis, we first investigated fiber sizes ranging from 270 nm to 1.04 μm by changing the concentration of TSPU from 8 to 14% during electrospinning (fig. S2, A and B). Histological examination of devices with different fiber sizes implanted in I.P. space for 4 weeks revealed that devices with a fiber size below ~500 nm had no cell penetration and induced only thin (<10 μm) cellular overgrowth, whereas those above 500 nm allowed cell penetration (fig. S2C). Then, we tested devices made from a different material (nylon) for comparison. With a similar fiber size (~250 nm), the nylon devices also prevented cell penetration after 4 weeks of I.P. implantation (fig. S2, A and C), but the delamination of different layers in the nanofiber membrane was observed (fig. S2C). These results confirmed that the TSPU nanofibrous device with proper nanofiber sizes was uniquely suitable for cell encapsulation.

Protection of syngeneic/allogeneic cells and confinement of proliferative cells

The ability of a cell encapsulation device to prevent cell escape is of paramount importance in SC-β cell delivery due to risks of teratoma formation from undifferentiated cells. However, too tight pore structures will diminish the mass transfer that is necessary for cell viability and function. To test whether the NICE device can provide a solution to the safety/function balance, we encapsulated and implanted luciferase-expressing cells and continuously monitored them over time in C57BL/6 mice. First, syngeneic mesenchymal stem cell (MSC) aggregates (~100 to 150 μm in diameter) with green fluorescent protein (GFP)/luciferase expression (fig. S3A) were encapsulated in NICE devices and implanted in the I.P. space. The bioluminescent signals were localized to the implantation site during the duration (5 months) of implantation and remained steady after an initial drop (Fig. 3, A and B). No signal was detected in the recipient animals after device retrieval (Fig. 3A), whereas the retrieved devices were bioluminescent (Fig. 3C), suggesting that the cells were confined and viable in the NICE device for 5 months. To confirm these imaging results, we also performed histological analysis on retrieved samples. H&E images showed the confinement and viability of the MSC aggregates within the device (Fig. 3D).

Next, allogeneic GFP/luciferase islets with a size of about 100 to 150 μm (fig. S3B) were monitored within the device over time. It was found that 48.9% radiance was detected on day 10 compared to day 1 (Fig. 3E), similar to the initial signal drop in the MSC case. The acute loss of encapsulated cells after implantation was considered common and most likely caused by hypoxia (*34*, *35*). However, there was no significant difference ($P = 0.7798$) among days 10, 30, 60, 90, and 120, which demonstrated that the islets remained stable after 10 days (Fig. 3, E and F). Postretrieval imaging of the recipients and devices (Fig. 3, E and G) as well as H&E and insulin/glucagon staining confirmed the robust function of the islets after 120 days (Fig. 3H and fig. S3).

To challenge our device, we tested whether it could protect invasive cells with a metastatic phenotype and prevent them from escaping. Allogeneic cancer cell spheroids (4T1) with GFP/luciferase expression (fig. S3C) were encapsulated in the NICE device. In two of the six mice, the bioluminescent signal disappeared after 2 weeks, suggesting early failure possibly due to unintentional defects of the device and/or biological variation. However, in the other four mice, the signal increased significantly ($P < 0.0001$) after 60 days and lasted for up to 150 days, indicating that the cells were protected (i.e., no immune cell penetration) and proliferated in the device (Fig. 3, I and J). In all cases, no bioluminescence outside the implantation site or device was observed. The imaging of retrieved device and H&E staining confirmed that the NICE device was able to support cell viability and prevent them from escape (Fig. 3, K and L). Another GFP/luciferase-expressing, allogeneic cell line, NIT-1 β

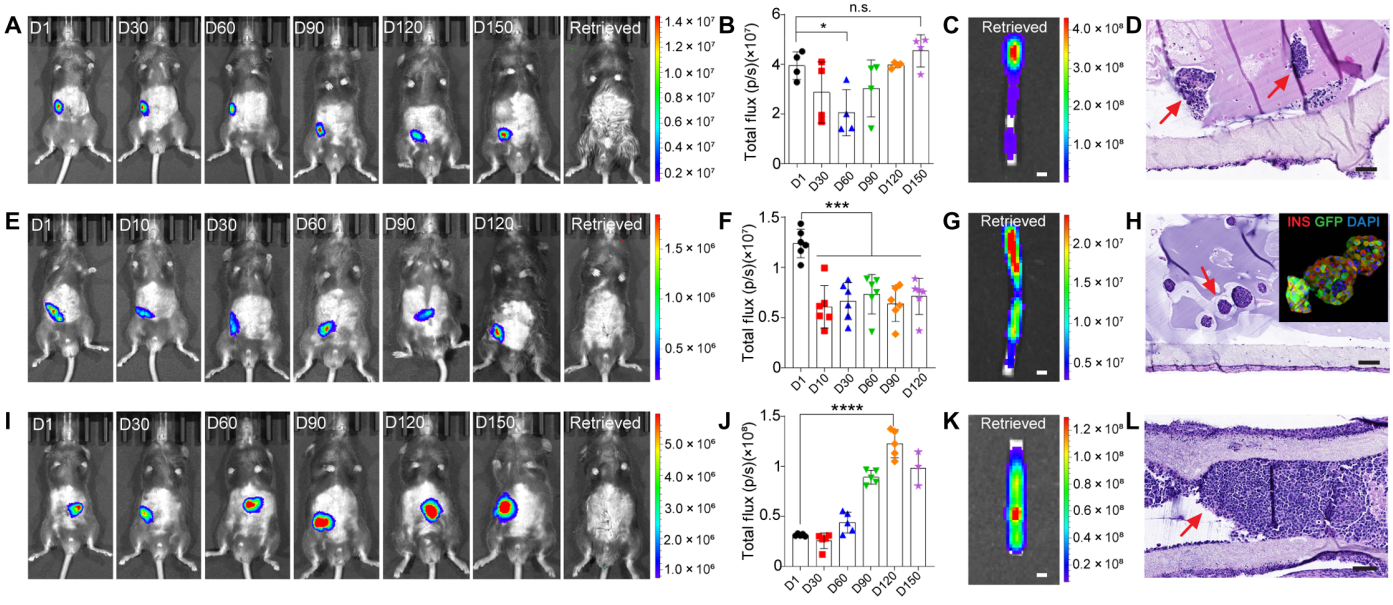

Fig. 3. Survival and confinement of different types of cells within the device. (**A**) Representative bioluminescent images of healthy C57BL/6 mice transplanted with NICE devices encapsulating GFP/luciferase-expressing syngeneic MSC spheroids for up to 150 days (from left to right are days 1, 30, 60, 90, 120, and 150) and after retrieval (far right). (**B**) Quantitative analysis of the bioluminescence intensity of the device; mean ± SD ($n = 4$). (**C**) A representative bioluminescent image of retrieved device. (**D**) H&E staining of a retrieved device at day 150. Arrows point to the MSC spheroids. (**E**) Representative bioluminescent images of healthy C57BL/6 mice transplanted with NICE devices encapsulating FVB GFP/luciferase mouse islets for up to 120 days (from left to right are days 1, 10, 30, 60, 90, and 120) and after retrieval (far right). (**F**) Quantitative analysis of the bioluminescence intensity of the device; mean ± SD ($n = 6$). (**G**) A bioluminescent image of a retrieved device. (**H**) H&E staining of a retrieved device. Arrow points to the mouse islets. The top-right corner shows immunofluorescent staining of mouse islets transplanted for 120 days (red, INS; green, GFP; and blue, DAPI). (**I**) Representative bioluminescent images of healthy C57BL/6 mice transplanted with NICE devices encapsulating BALB/c GFP/luciferase 4T1 spheroids for up to 150 days (from left to right are days 1, 30, 60, 90, 120, and 150) and after retrieval (far right). (**J**) Quantitative analysis of the bioluminescence intensity of the device; mean ± SD ($n = 5$). (**K**) A bioluminescent image of a retrieved device. (**L**) H&E staining of a retrieved device. Arrow points to the 4T1 cells encapsulated in device for 120 days. The data were compared using one-way ANOVA followed by Tukey's multiple comparisons test. *$P < 0.05$, ***$P < 0.001$, and ****$P < 0.0001$; n.s., nonsignificant. Scale bars, 1 mm (C, G, and K) and 100 μm (D, H, and L). GFP, green fluorescent protein; MSC, mesenchymal stem cell; INS, insulin.

cell spheroids, were also confined and protected by the NICE device for 2 months (fig. S3G). Together, these data showed that the NICE device was cell protective and safe.

Diabetes correction in mice with diverse rodent islet sources

To investigate the function of the NICE device in reversing diabetes, we encapsulated the different types of rodent islets (syngeneic, allogeneic, and xenogeneic) in the device and implanted it in diabetic C57BL/6 mice. Rodent islets were dispersed evenly and embedded in alginate in the NICE device before transplantation. With 600– to 700–islet equivalent (IEQ) syngeneic islets, the NICE device corrected diabetes in 13 of 17 mice. The engrafted mice maintained blood glucose within a normal range until device retrieval for as long as 120 days (Fig. 4A). The device encapsulating allogeneic BALB/c islets (600 to 700 IEQ) engrafted in 16 of 24 mice, with function for up to 200 days (Fig. 4B). Increasing immunological incompatibility of the transplanted cells by using rat islets (600 to 700 IEQ) demonstrated function for longer than 100 days (Fig. 4C). In all engrafted animals, the blood glucose concentration dropped within a week of transplantation and increased after graft retrieval at different time points (Fig. 4, A to C), confirming that the glucose concentrations were controlled by the grafts. The devices were easily retrievable and there was no tissue adhesion in most cases. The increased body weight of all engrafted mice, similar to healthy mice, showed metabolic recovery, whereas that of diabetic mice dropped continuously (Fig. 4D).

To evaluate the metabolic control of blood glucose, we performed an I.P. glucose tolerance test (IPGTT) on day 30. The IPGTT measurements indicated that all engrafted mice cleared glucose 2 hours after bolus, similar to healthy mice, whereas the peak value of blood glucose after stimulation in engrafted mice was higher than that of healthy mice. The rate of glucose clearance in all the engrafted mice was significantly ($P < 0.05$) faster than that of the diabetic group (Fig. 4E). Quantitatively, the area under curve (AUC) for glucose clearance in the engrafted mice receiving syngeneic, allogeneic, and xenogeneic islets was similar to the healthy mice (Fig. 4F). There was no difference ($P = 0.1516$) in the AUC among the engrafted mice implanted with different sources of islets. The IPGTT carried out on the engrafted mice with grafts lasting over 4 months also indicated long-term function (fig. S4). To provide additional proof that the transplanted islets were responsible for glucose control, we carried out an ex vivo GSIS test (Fig. 4G). The responsiveness of islets inside the device indicated their viability and normal function. Last, an about 60× decrease of insulin content in the pancreas of engrafted mice compared to healthy mice confirmed again that the streptozotocin (STZ) induction had successfully depleted the β cells in pancreas and that the transplanted grafts were responsible for the observed metabolic control (Fig. 4H).

Allogeneic islets in devices retrieved after 40 days appeared healthy, similar to those before transplantation (Fig. 4I). The histological studies showed no tissue adhesion around the device and no cell penetration into the device (Fig. 4, J to O). Quantitative analysis of the cellular overgrowth in H&E staining images showed that although there was a relatively thicker fibrotic layer (~30 μm) for xenografts, the fibrotic deposition was minimal (about 10 μm in thickness) for autografts and allografts (Fig. 4P). Islets from different sources encapsulated within the device were viable in the short term (<40 days) (Fig. 4, J to L, and fig. S5, A to C) and in the long term (>100 days) (Fig. 4, M to O). Moreover, islets inside the device were morphologically normal with a round shape, even at long time points (170 days) with a high density in an allogeneic environment (Fig. 4N). Immunofluorescent staining for insulin and glucagon demonstrated that cells maintained their individual hormone identities, many of which were insulin-expressing β cells (Fig. 4, J to O). Quantitative analysis of the expression of insulin and glucagon after transplantation showed that on average, about 80% of the cells within one islet were insulin-expressing β cells and 15% of cells were glucagon-expressing α cells in autografts and allografts (Fig. 4Q), which were similar to the percentages of α and β cells before transplantation (fig. S5D). About 88% of insulin$^+$ cells and ~10% of glucagon$^+$ cells were observed in rat islets after transplantation, also similar to those before transplantation (Fig. 4Q and fig. S5D). Together, these data demonstrated that the NICE device was biocompatible and long-term functional in correcting diabetes in mice with diverse rodent islets.

Immunoprotective function of NICE device in autografts, allografts, and xenografts

To analyze the immune responses and understand the immunoprotective function of the device under different transplantation scenarios (i.e., autografts, allografts, and xenografts), we retrieved the devices after 1 month of implantation and analyzed for the cellular composition surrounding the device and the antibodies within the device. Flow cytometry analysis of the cells deposited on the device showed that 25% of the cells surrounding the encapsulation device were immune cells in the autograft group (Fig. 5A). In contrast, 80% of the cells deposited on the device were immune cells in allografts and xenografts, most of which were CD3$^+$ or CD4$^+$ T cells and macrophages (Fig. 5, A to C, and figs. S6 and S7A). Less than 1.5% of cells were CD8$^+$ T cells, which suggested that CD8$^+$ T cells were not recruited to the graft (Fig. 5D). Other types of immune cells found in the fibrotic layer included B cells (about 5%), neutrophils (less than 5%), and dendritic cells (about 15%) (fig. S7, B to D). These data showed that despite the presence of various types of immune cells, there were very few CD8$^+$ T cells around the device even in xenografts.

To study the humoral immune response to the encapsulated cells, we analyzed the mouse total antibodies [immunoglobulin G (IgG) and IgM] in serum at different time points after transplantation, in I.P. fluid, and inside the device after retrieval. Mouse IgG antibody in xenografts increased significantly ($P < 0.05$) over the 4-week period, whereas it changed slightly in autografts and allografts (Fig. 5E). Elevated IgM antibodies were observed in the mouse serum in xenografts as early as 7 days after transplantation, with slight decrease at 2 weeks and another peak at 3 weeks (Fig. 5F). Different from xenografts, IgM increased over time in allografts (Fig. 5F). Moreover, it appeared that the antibody response slightly increased in the mice with devices encapsulating xenogeneic islets relative to those with devices encapsulating syngeneic or allogeneic islets (Fig. 5, E and F). This response could be elicited by antigens shed from inside the device. The mouse total antibody (IgG and IgM) concentrations in the devices were significantly ($P < 0.05$) lower than those in I.P. fluids in all grafts including xenografts (Fig. 5, G and H). To determine whether the IgG and IgM detected in allografts were donor-specific alloantibodies, we incubated the BALB/c T cells with serum withdrawn from the recipients with allografts and labeled with fluorescein isothiocyanate anti-mouse IgG or anti-mouse IgM. Serum extracted from sensitized C57BL/6 mice

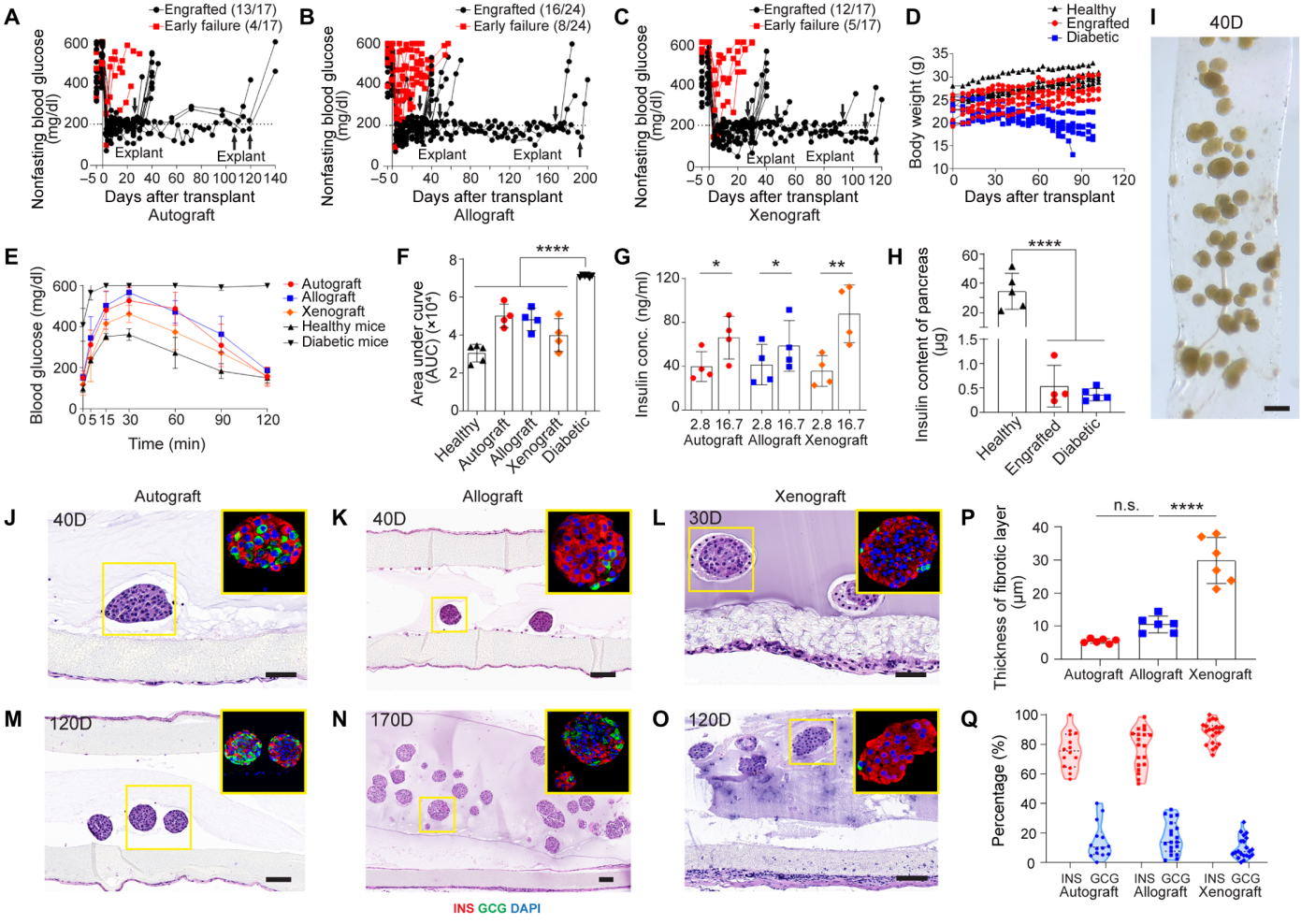

Fig. 4. Device function with syngeneic, allogeneic, and xenogeneic islets in diabetic immunocompetent C57BL/6 mice. (**A** to **C**) Nonfasting blood glucose concentrations of the recipient mice transplanted with syngeneic mouse islets ($n = 17$) (A), allogeneic mouse islets ($n = 24$) (B), and xenogeneic rat islets ($n = 17$) (C). Arrows indicate the time points when implants were retrieved from recipients. (**D**) Body weights of healthy, engrafted, and diabetic mice measured for up to 105 days ($n = 5$). (**E**) Measurement of blood glucose in IPGTT in different groups on day 30; mean ± SD ($n = 5$ for healthy mouse group, $n = 4$ for engrafted groups, and $n = 6$ for diabetic mouse group). (**F**) Quantification of AUC from (E) for different groups on day 30; mean ± SD. (**G**) Measurement of insulin concentration of retrieved devices from engrafted mice in different groups after ex vivo GSIS test; mean ± SD ($n = 4$). (**H**) Measurement of total insulin content of the pancreas in different groups; mean ± SD ($n = 4$ to 5). (**I**) Bright-field image of encapsulated mouse islets retrieved from allogeneic transplantation model on day 40. (**J** and **K**) H&E staining and immunofluorescent staining (shown in inset) of syngeneic islets (J) and allogeneic islets (K) from device retrieved after 40 days (red, INS; green, GCG; and blue, DAPI). (**L**) H&E staining and immunofluorescent staining (shown in inset) of xenogeneic rat islets from retrieved device after 30 days (red, INS; green, GCG; and blue, DAPI). (**M**) H&E staining and immunofluorescent staining (shown in inset) of syngeneic islets from retrieved device after 120 days (red, INS; green, GCG; and blue, DAPI). (**N**) H&E staining and immunofluorescent staining (shown in inset) of allogeneic islets from retrieved device after 170 days (red, INS; green, GCG; and blue, DAPI). (**O**) H&E staining and immunofluorescent staining (shown in inset) of xenogeneic islets from retrieved device after 120 days (red, INS; green, GCG; and blue, DAPI). (**P**) Quantification of the thickness of fibrotic layer in three different groups: autograft, allograft, and xenograft at 1 month. (**Q**) Percentage of hormone expression (insulin and glucagon) quantified from immunofluorescent staining images of encapsulated islets retrieved from three different groups: autograft, allograft, and xenograft. One point represents one islet. The two-tailed Student's *t* test was performed when the data consisted of only two groups. The one-way ANOVA followed by Tukey's test was performed for comparing the multigroup data. $^*P < 0.05$, $^{**}P < 0.01$, and $^{****}P < 0.0001$; n.s., nonsignificant. Scale bars, 200 μm (I), 100 μm (K, M, N, and O), and 50 μm (J and L). IPGTT, intraperitoneal glucose tolerance test; AUC, area under curve; GSIS, glucose stimulation insulin secretion; H&E, hematoxylin and eosin; INS, insulin; GCG, glucagon.

with BALB/c islets transplanted in kidney capsules at 4 weeks after transplantation was used as positive control. The flow cytometry data showed that there were anti-BALB/c alloantibodies (IgG and IgM) detected in C57BL/6 serum with allografts at 28 days after transplantation, although with much lower concentration than in the serum of sensitized mice (fig. S8). However, almost no alloantibodies were present inside the device (fig. S8). These data confirmed the immunoprotective function of the device.

The NICE device supports the function of human islets in immunodeficient mice

To demonstrate the potential of the NICE device for human islet encapsulation, we performed transplantation in diabetic, severe combined immunodeficient (SCID)–beige mice. Human islets with variable sizes but acceptable viability (70 to 90%) (Fig. 6A and fig. S9A) were received, encapsulated (~1700 IEQ per mouse), and transplanted. From immunofluorescent staining studies, before

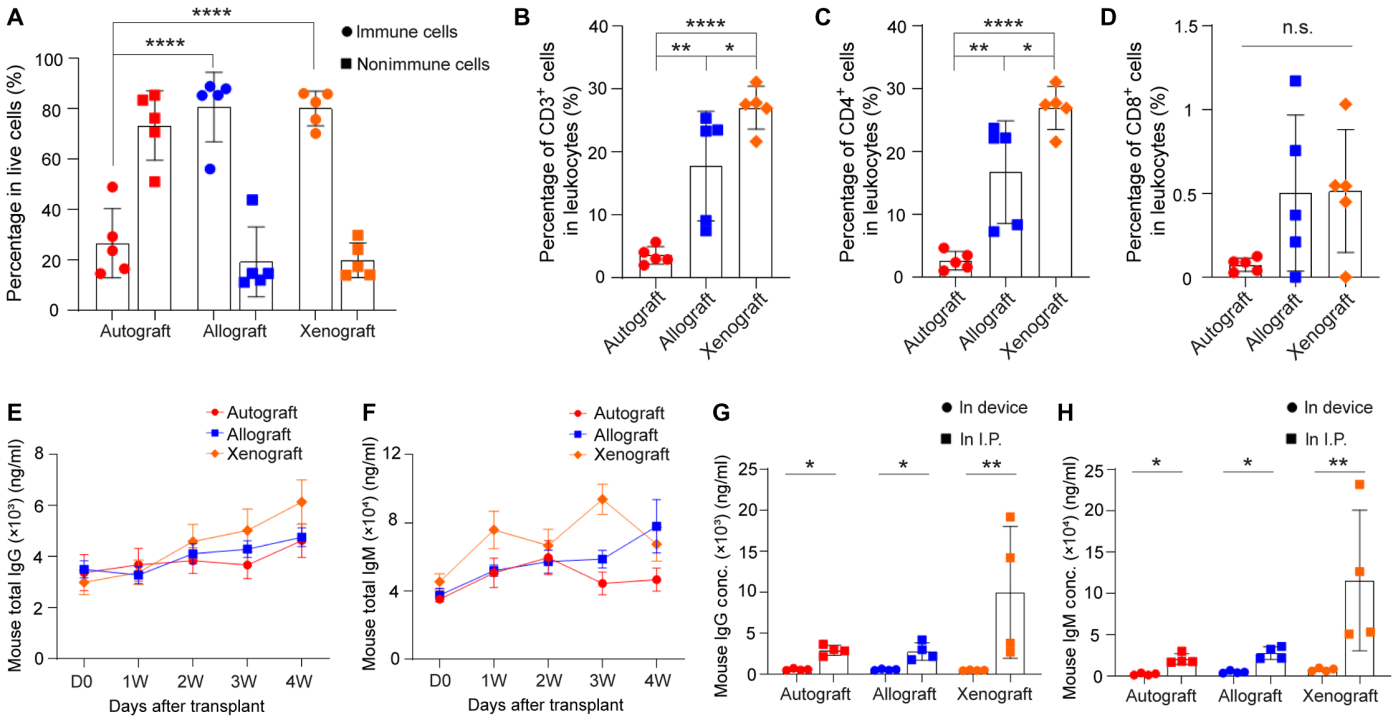

Fig. 5. Immunoprotective function of the device. Analysis of immune cells in the fibrotic layer around the NICE device (A to D) and antibody concentrations (E to H) in three different groups: autograft, allograft, and xenograft. (**A**) Percentage of immune cells and nonimmune cells in live cells; mean ± SD ($n = 5$). (**B**) Percentage of $CD3^+$ cells in leukocytes; mean ± SD ($n = 5$). (**C**) Percentage of $CD4^+$cells in leukocytes; mean ± SD ($n = 5$). (**D**) Percentage of $CD8^+$ cells in leukocytes; mean ± SD ($n = 5$). (**E**) Measurement of mouse total IgG in serum extracted from recipients with autografts (red line), allografts (blue line), and xenografts (orange line) before transplantation and at 1, 2, 3, and 4 weeks after transplantation; mean ± SD ($n = 5$). (**F**) Measurement of mouse total IgM in serum extracted from recipients with autografts (red line), allografts (blue line), and xenografts (orange line) before transplantation and at 1, 2, 3, and 4 weeks after transplantation; mean ± SD ($n = 5$). (**G**) Measurement of mouse IgG in retrieved device and in I.P. fluid extracted from recipients after device retrieval; mean ± SD ($n = 4$). (**H**) Measurement of mouse IgM in retrieved device and in I.P. fluid extracted from recipients after device retrieval; mean ± SD ($n = 4$). The two-tailed Student's *t* test was performed when the data consisted of only two groups. The one-way ANOVA followed by Tukey's test was performed for comparing the multigroup data. *$P < 0.05$, **$P < 0.01$, and ****$P < 0.0001$; n.s., nonsignificant.

transplantation, the human islets expressed β cell markers such as insulin, C-peptide, and transcription factor NKX6.1 (fig. S9, B and C). Eight of the 11 recipient mice recovered from diabetes immediately (within a week) and maintained normoglycemia for up to 100 days before device retrieval (Fig. 6B). Human C-peptide after IPGTT at 2-, 8-, and 14-week time points was detectable in the serum, and the concentration was significantly ($P < 0.05$) increased at 90 min compared to 0 min (Fig. 6C), suggesting that human islets inside the device were responsive to glucose and secreted insulin. Blood glucose measurements during an IPGTT at week 8, representative of other time points, showed that the engrafted mice cleared glucose within 2 hours (Fig. 6D). The retrieved device had minimal cellular overgrowth, and healthy islets were observed in the device in both the short term (Fig. 6, E to G) and long term (Fig. 6, H to J). Immunofluorescent staining showed insulin and glucagon expression (Fig. 6, F and I) and C-peptide and NKX6.1 expression (Fig. 6, G and J) at 40 and 105 days, although some small necrotic areas were present in larger islets. Quantitative analysis of the expression of insulin and glucagon after transplantation showed that about 64% of cells within one islet were insulin-expressing β cells and 31% of cells were glucagon-expressing α cells (Fig. 6K), which were similar to the percentages of α and β cells of human islets before transplantation (fig. S9D). In addition, no polyhormonal cells were observed either before or after transplantation. Further analysis revealed that about 67% of cells within one islet were C-peptide$^+$ cells, 55% of cells were NKX6.1$^+$, and 54% were C-peptide$^+$/NKX6.1$^+$ β cells (Fig. 6L), which were also similar to those before transplantation (fig. S9E). To further verify that the transplanted islets were responsible for glucose control, we retrieved the engrafted devices 1 month after implantation and carried out an ex vivo GSIS test. The retrieved devices secreted significantly ($P < 0.05$) more human C-peptide in high-glucose solution than that in low-glucose solution (Fig. 6M). In addition, dynamic calcium imaging was conducted on extracted, dissociated single cells. The cells responded with the increased calcium influx when exposed to high-glucose solution or potassium chloride (KCl), an agent to depolarize the cell membrane (Fig. 6N), confirming their functions.

The NICE device supports the function of human SC-β cells in immunodeficient mice

From a broad point of view, the highest impact of a cell encapsulation device that is both safe and functional would be its use for delivery of human SC-β cells. To provide evidence that the NICE device has this potential, we first encapsulated human SC-β cells (*6*, *9*) and implanted them in diabetic immunodeficient NOD. Cg-*Prkdc*^{scid} *Il2rg*^{tm1Wjl}/SzJ (NSG) mice (~2500 clusters per mouse). The SC-β cells had a more uniform size (~100 to 150 μm in diameter) compared to the human islets (Fig. 7A). From immunofluorescent

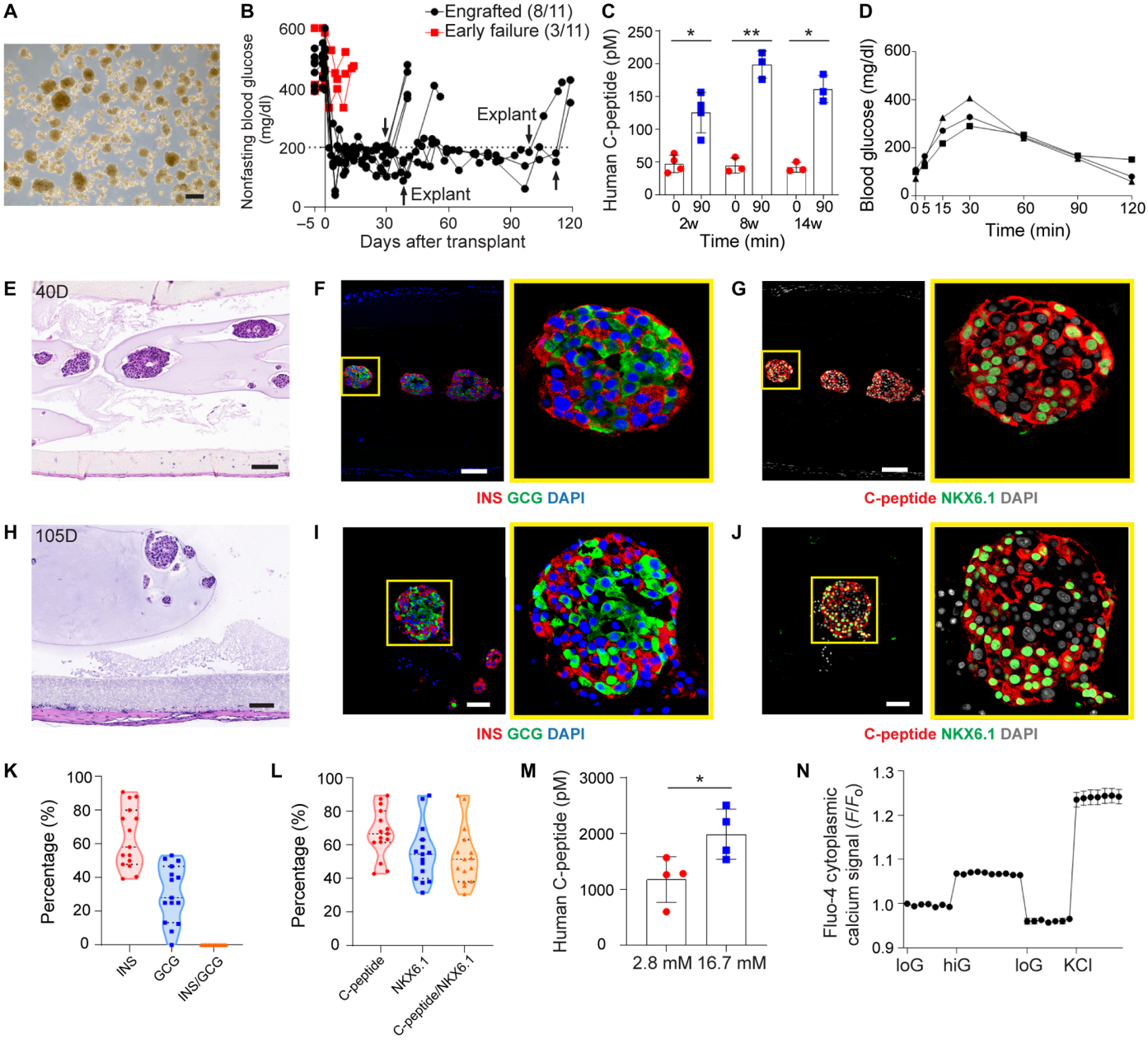

Fig. 6. Device function with human islets in diabetic immunodeficient SCID-beige mice. (**A**) Bright-field image of human islets before transplantation. (**B**) Measurement of nonfasting blood glucose ($n = 11$). Arrows indicate the time points when implants were retrieved from recipients. (**C**) Measurement of human C-peptide in serum of the mice at 0 and 90 min after IPGTT after 2, 8, and 14 weeks of transplantation; mean ± SD ($n = 3$ to 4). (**D**) Typical blood glucose measurement in IPGTT of engrafted recipients (week 8). (**E** to **G**) H&E staining (E) and immunofluorescent staining (F and G) of human islets from retrieved device after 40 days (higher magnifications on the right). (**H** to **J**) H&E staining (H) and immunofluorescent staining (I and J) of human islets from retrieved device after 105 days (higher magnifications on the right). (F and I) Coimmunofluorescent staining of insulin (INS; red), glucagon (GCG; green) and DAPI (blue). (G and J) Coimmunofluorescent staining of C-peptide (red), NKX6.1 (green), and DAPI (gray). (**K**) Percentage of hormone expression (insulin, glucagon, and insulin/glucagon) quantified from immunofluorescent staining images. One point represents one islet ($n = 15$). (**L**) Percentage of β cell marker expressions (C-peptide, NKX6.1, and C-peptide/NKX6.1) quantified from immunofluorescent staining images. One point represents one islet ($n = 15$). (**M**) Measurement of C-peptide concentration of retrieved devices from engrafted mice after ex vivo GSIS test; mean ± SD ($n = 4$). (**N**) Measurements of dynamic normalized Fluo-4 fluorescence intensity for retrieved human islets challenged sequentially with 2, 20, and 2 mM glucose and 30 mM KCl; mean ± SEM ($n = 11$). The two-tailed Student's t test was performed when the data consisted of two groups. $^*P < 0.05$ and $^{**}P < 0.01$. Scale bars, 200 μm (A), 100 μm (E to H), and 50 μm (I and J). IPGTT, intraperitoneal glucose tolerance test; H&E, hematoxylin and eosin; INS, insulin; GCG, glucagon; GSIS, glucose stimulation insulin secretion; KCl, potassium chloride.

staining studies, before transplantation, the SC-β cells expressed β cell markers such as insulin, C-peptide, and NKX6.1 (fig. S10, A and B). About 60% of cells expressed both C-peptide and NKX6.1 as measured by flow cytometry (Fig. 7B), and 12% were polyhormonal cells with expression of both C-peptide and glucagon (Fig. 7C). Slightly lower C-peptide expression (~55%) was obtained by quantifying the immunofluorescent staining images (fig. S10, C and D). In a dynamic GSIS assay, SC-β cells secreted higher amounts of insulin with a clear first- and second-phase response when exposed to increased glucose (Fig. 7D). Static GSIS also demonstrated that before transplantation, SC-β cells can secrete more insulin in high-glucose solution than that in low-glucose solution (fig. S10E). Furthermore, oxygen consumption rate (OCR) measurement showed that SC-β cells had a higher OCR normalized to DNA than human islets, indicating that SC-β cells might have a higher metabolism than human islets (Fig. 7E).

The device with SC-β cells corrected blood glucose immediately (within a week) in 11 of 16 mice, which was maintained for up to 120 days (Fig. 7F). Recipients became diabetic again after explanting the devices, showing that blood glucose was controlled by the NICE device with SC-β cells (Fig. 7F). Human C-peptide in the blood at 90 min after glucose challenge (111 ± 21.3 pM) was significantly ($P < 0.05$) higher than the fasting value (21.4 ± 7.7 pM) 2 weeks after implantation (Fig. 7G). At 8 weeks, there was also glucose-responsive C-peptide secretion at 90 min (151.2 ± 15.4 pM) compared to that at 0 min (34.8 ± 3.1 pM) (Fig. 7G). There was no significant difference ($P = 0.4511$) in terms of the SI at 2 weeks (5.4 ± 1.9) and that at 8 weeks (4.3 ± 0.1), suggesting stable device function during that period (fig. S10F). For the engrafted mice studied at 30 days, glucose clearance after IPGTT was completed by 120 min (Fig. 7H); the AUC of the glucose concentration curve was similar to that of healthy mice, although significantly ($P < 0.01$) less than that of diabetic mice (Fig. 7, H and I). An IPGTT study carried out at 8 weeks also demonstrated the long-term function of SC-β cells in the device (fig. S10G). In addition, the total insulin content in the pancreas of the engrafted mice was significantly ($P < 0.0001$) lower than that of healthy mice, which again confirmed that the transplanted grafts were responsible for the observed metabolic control (fig. S10H).

Ex vivo GSIS test showed that devices retrieved at 1 month secreted significantly ($P < 0.05$) more human C-peptide in high-glucose solution than that in low-glucose solution (Fig. 7J). Dynamic calcium imaging conducted on dissociated cells corroborated the GSIS results: The retrieved SC-β cells exhibited glucose- and KCl-responsive calcium influx (Fig. 7K). SC-β cells explanted after 40 and 120 days remained viable with a healthy and round morphology, although the cells were packed at a high density within the device (Fig. 7L). The expression of insulin, glucagon, C-peptide, and NKX6.1 of the cells retrieved at different time points (up to 120 days) indicated device function in both short and long terms (Fig. 7 and fig. S11). Quantitative analysis of the hormone expression within each cell aggregate after transplantation averaged over four recipients showed that about 38% of cells were insulin-expressing β cells and 34% of cells were glucagon-expressing α cells (Fig. 7S). Polyhormonal cells were observed before transplantation, but less than 1% of cells expressed both insulin and glucagon after retrieval (Fig. 7). About 43% of cells within one aggregate expressed C-peptide, 37% of cells expressed NKX6.1, and 19% expressed both markers (Fig. 7T). About 32% of cells within the device expressed MAF BZIP Transcription Factor A (MAFA), a maturation marker of β cells, after transplantation (fig. S12). The decline of C-peptide–expressing or insulin-expressing cells after transplantation may be due to the maturation of polyhormonal cells observed before transplant into α cells in vivo (*6*, *7*). Despite a lower percentage of β cells, the percentage of α cells in SC-β cells was similar to that in human islets; α cells are important in the cross-talk with β cells and controlling blood glucose concentration (*36*, *37*). These results show that the NICE device supported the function of the human SC-β cells in immunodeficient mice.

Testing of the NICE device with human SC-β cells in immunocompetent models

After confirming the function of encapsulated human SC-β cells in immunodeficient mice, we explored the use of the NICE device for delivering cells in immunocompetent diabetic mice and healthy dogs. It is noted that these xenotransplantation models may be more challenging than allogeneic, human SC-β cells–to–human transplantation, and the explorations here are intended to test the robustness, safety, scalability, and retrievability in the setting of SC-β cell delivery but not necessarily the full, long-term function of the device. Nevertheless, when devices with the human SC-β cells (~2500 clusters) were implanted in diabetic C57BL/6 mice, 10 of 16 mice became normoglycemic immediately (within a week) after transplantation and maintained normoglycemia for up to 8 weeks (Fig. 8A), a result better than anticipated. Human C-peptide in the blood of mice with engrafted SC-β cells at 90 min after glucose challenge (86.7 ± 10.4 pM) was significantly ($P < 0.01$) higher than the fasting value (12.4 ± 1.1 pM) 2 weeks after implantation (Fig. 8B). However, at 4 weeks, there was no significant difference ($P = 0.11$) in C-peptide secretion before and after glucose injection, which indicated that the function of cells declined after 4 weeks (Fig. 8B). Blood glucose measurement during IPGTT at 2 weeks showed that the engrafted mice cleared glucose within 2 hours, whereas the mice with early failed grafts remained at high glucose concentrations (Fig. 8C). The mice engrafted with SC-β cells showed blood glucose clearance after IPGTT similar to those engrafted with human islets (Fig. 8C), which were included as a control (fig. S13). The SC-β cells in retrieved devices secreted significantly ($P < 0.001$) more human C-peptide in high-glucose solution than that in low-glucose solution after ex vivo GSIS test (Fig. 8D). In addition, the dynamic calcium imaging conducted on retrieved cells showed glucose-responsive calcium influx (Fig. 8E). Histological studies showed that the SC-β cells were reasonably healthy after 35 days, despite the formation of a more severe FBR than that observed in immunodeficient mice and the presence of some cells having penetrated into the membrane (Fig. 8F and fig. S14). Immunofluorescent staining also confirmed the expression of insulin, glucagon, C-peptide, NKX6.1 (Fig. 8, G and H, and fig. S15), and MAFA. It is noted that human SC-β cells elicited much stronger ($P < 0.01$) immune responses than rodent islets in mice (fig. S16). Applying immunosuppression, such as treatment of rapamycin that suppresses T cell activation and proliferation, led to improved engraftment of encapsulated SC-β cells in immunocompetent mice (fig. S17).

To support the concept that the NICE device is scalable, easy to handle and implant, and retrievable, we implanted devices containing human SC-β cells into healthy dogs ($n = 3$) without administering immunosuppressive drugs. We loaded a subtherapeutic dose (2500 clusters) of SC-β cells into 1-mm-diameter, 17-cm-long devices. In a typical procedure, the device was placed in a 10-ml

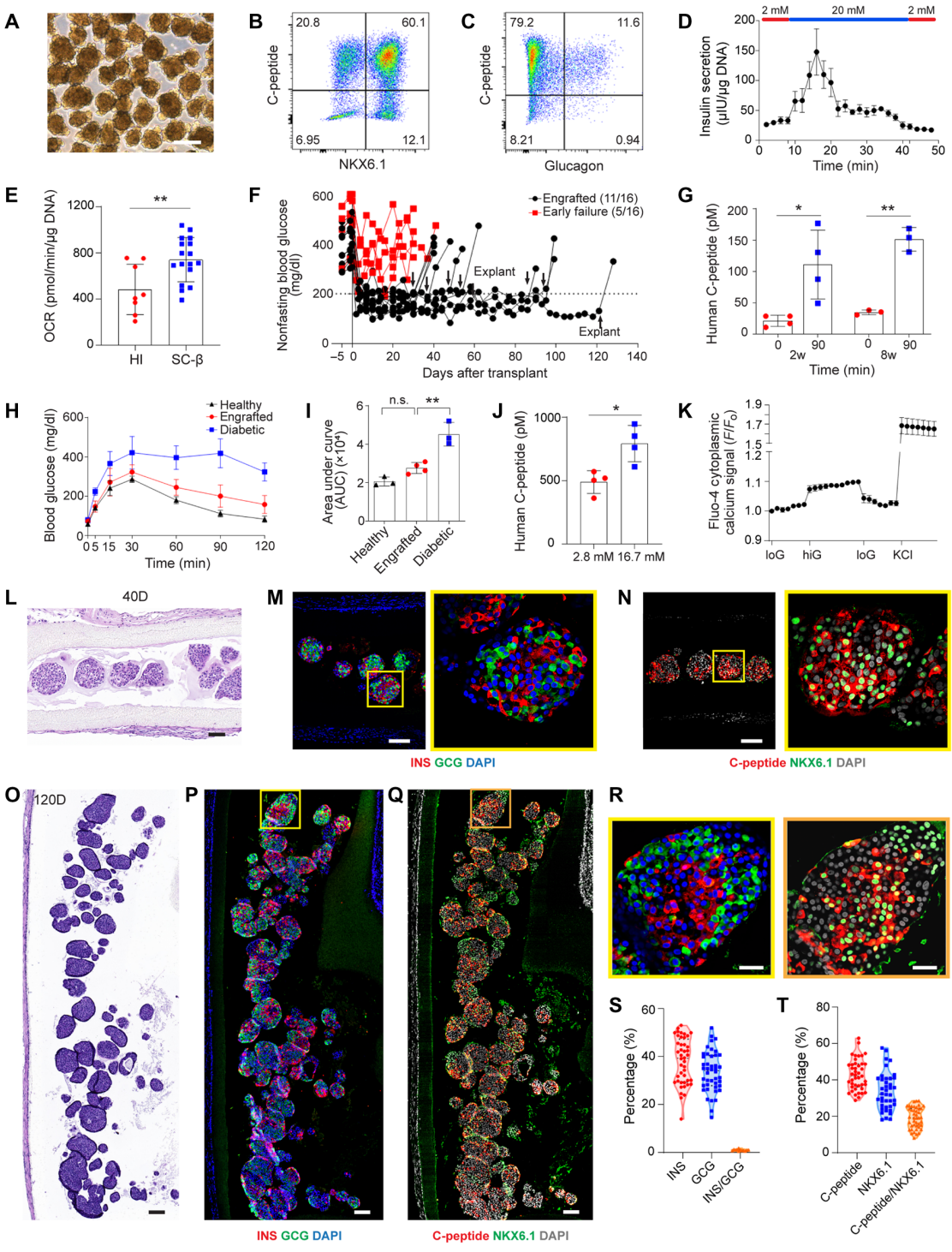

Fig. 7. Device function with SC-β cells in diabetic immunodeficient NSG mice. (**A**) Bright-field image of SC-β cell aggregates before transplantation. (**B** and **C**) Representative flow cytometric dot plots of dispersed stage 6 SC-β cells immunostained for the indicated markers. (**D**) Dynamic glucose-stimulated human insulin secretion of cells in stage 6 in a perfusion GSIS assay. Data for each individual time point are shown as means ± SEM ($n = 3$). Cells are perfused with low glucose (2 mM) and high glucose (20 mM) as indicated. (**E**) OCR of human islets (HI; $n = 8$) and SC-β cells ($n = 17$) at high glucose (20 mM) normalized to DNA content; mean ± SD. (**F**) Measurement of nonfasting blood glucose of the mice transplanted with SC-β cells in the device ($n = 16$). Arrows indicate the time points when implants were retrieved from recipients. (**G**) Measurement of human C-peptide in mouse serum at 0 and 90 min after IPGTT after 2 and 8 weeks of transplantation; mean ± SD ($n = 3$ to 4). (**H**) Representative blood glucose measurement in IPGTT of engrafted recipients ($n = 3$ to 4). (**I**) Quantification of AUC from (H) for different groups; means ± SD. (**J**) Measurement of C-peptide concentration of retrieved devices from engrafted mice after ex vivo GSIS test; mean ± SD ($n = 4$). (**K**) Measurements of dynamic normalized Fluo-4 fluorescence intensity for retrieved SC-β cells challenged sequentially with 2, 20, and 2 mM glucose and 30 mM KCl; mean ± SEM ($n = 14$). (**L** to **N**) H&E staining (L) and immunofluorescent staining (M and N) of SC-β cells from retrieved device after 40 days (higher magnification on the right). (**O** to **R**) H&E staining (O) and immunofluorescent staining (P to R) of SC-β cells from retrieved device after 120 days. (M and P) Coimmunofluorescent staining of insulin (red), glucagon (green), and DAPI (blue). (N and Q) Coimmunofluorescent staining of C-peptide (red), NKX6.1 (green), and DAPI (gray). (R) High-magnification images of cell aggregates from (P) and (Q). (**S**) Percentage of hormone expression (insulin, glucagon, and insulin/glucagon) per cell aggregate quantified from immunofluorescent staining images. One point represents one aggregate ($n = 44$). Samples were collected from four animals. (**T**) Percentage of β cell marker expressions (C-peptide, NKX6.1, and C-peptide/NKX6.1) per cell aggregate quantified from immunofluorescent staining images. One point represents one aggregate ($n = 43$). Samples were collected from four animals. The two-tailed Student's t test was performed when the data consisted of two groups. The one-way ANOVA followed by Tukey's test was performed for comparing the multigroup data. $^*P < 0.05$ and $^{**}P < 0.01$; n.s., nonsignificant. Scale bars, 250 μm (A), 100 μm (L to Q), and 25 μm (R). SC-β, stem cell–derived β cell; GSIS, glucose stimulation insulin secretion; IPGTT, intraperitoneal glucose tolerance test; AUC, area under curve; H&E, hematoxylin and eosin; INS, insulin; GCG, glucagon; KCl, potassium chloride.

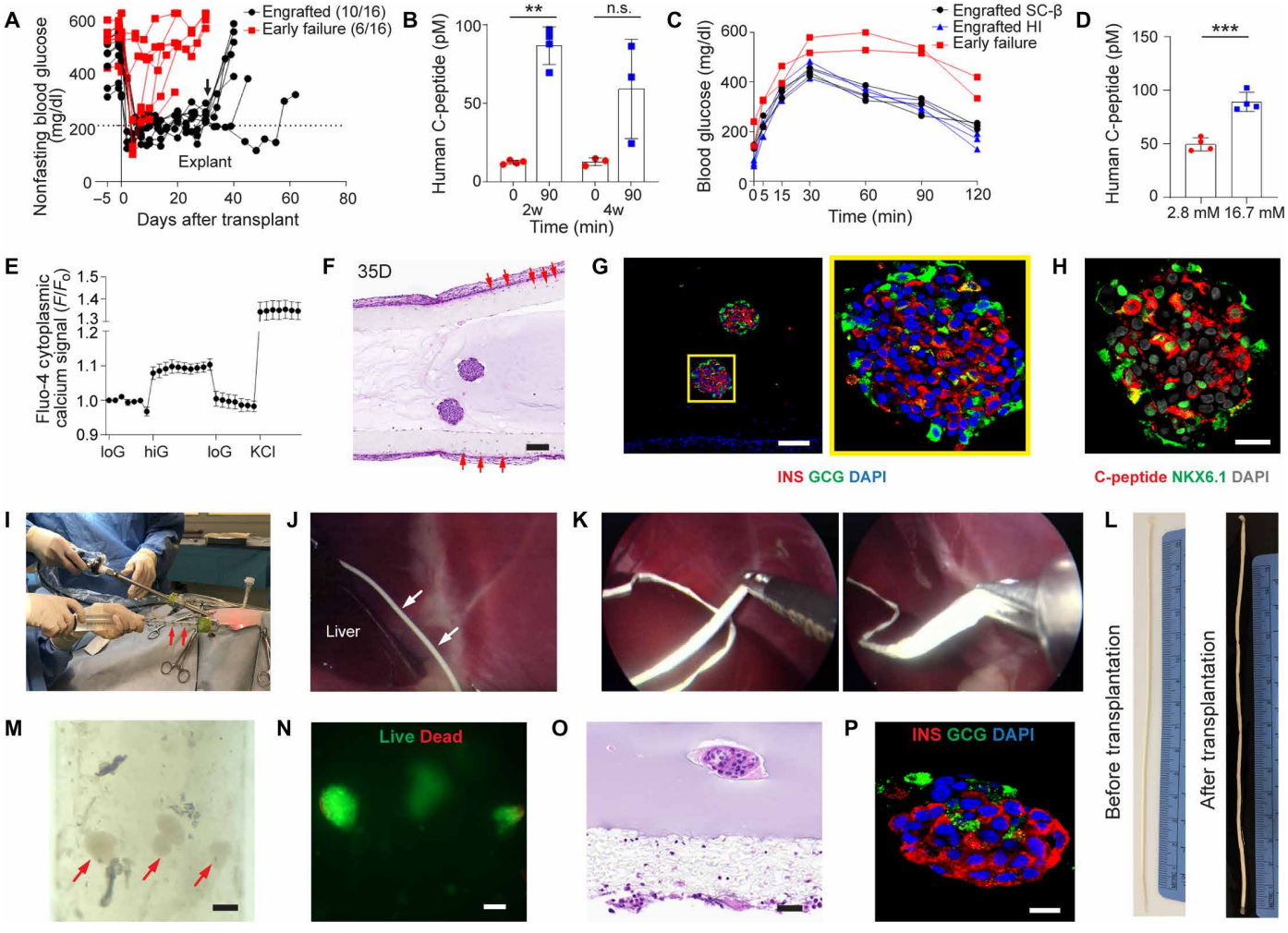

Fig. 8. Device function with SC-β cells in xenogeneic mouse and dog models. Device function with SC-β cells in diabetic immunocompetent C57BL/6 mice (A to H) and scalability, retrievability, and SC-β cell survival in healthy dogs (I to P). (**A**) Measurement of nonfasting blood glucose of the mice transplanted with SC-β cells in device ($n = 16$). Arrow indicates the time point when implants were retrieved from recipients. (**B**) Measurement of human C-peptide in mouse serum at 0 and 90 min after IPGTT after 2 and 4 weeks of transplantation; mean ± SD ($n = 3$ to 4). (**C**) Representative blood glucose measurement in IPGTT of engrafted recipients with human SC-β cells (black line), human islets (blue line), and failed human SC-β cells (red line) 14 days after transplant. (**D**) Measurement of C-peptide concentration of retrieved devices from engrafted mice after ex vivo GSIS test; mean ± SD ($n = 4$). (**E**) Measurements of dynamic normalized Fluo-4 fluorescence intensity for retrieved SC-β cells challenged sequentially with 2, 20, and 2 mM glucose and 30 mM KCl; mean ± SEM ($n = 6$). (**F** to **H**) H&E staining (F) and immunofluorescent staining (G and H) of SC-β cells from retrieved device after 35 days (higher magnification on the right). Red arrows in (F) indicated cells penetrating from outside to inside of the outer surface of the nanofibrous membrane. (G) Coimmunofluorescent staining of insulin (red), glucagon (green), and DAPI (blue). (H) Coimmunofluorescent staining of C-peptide (red), NKX6.1 (green), and DAPI (gray). (**I**) Photograph showing the laparoscopic implantation of device ($n = 3$). Red arrows point to the device in a 10-ml pipette during implantation. (**J**) Laparoscopic image showing the device implanted in I.P. space near the liver in a dog. White arrows point to the device. (**K**) Laparoscopic images showing the device being pulled out from a dog during retrieval. (**L**) Photograph of a device before transplantation and a device retrieved from a dog after 2 weeks. (**M**) Bright-field image of encapsulated SC-β cells after retrieval (red arrows point to SC-β cells). (**N**) Live (green) and dead (red) staining of the SC-β cells in (M). (**O** and **P**) H&E staining (O) and immunofluorescent staining (P) of SC-β cells from retrieved device after 2 weeks. (P) Coimmunofluorescent staining of insulin (red), glucagon (green), and DAPI (blue). The two-tailed Student's *t* test was performed. $^{**}P < 0.01$ and $^{***}P < 0.001$; n.s., nonsignificant. Scale bar, 100 μm (F, G, M, and N), 50 μm (O), and 25 μm (H and P). SC-β, stem cell–derived β cell; IPGTT, intraperitoneal glucose tolerance test; GSIS, glucose stimulation insulin secretion; KCl, potassium chloride; H&E, hematoxylin and eosin; INS, insulin; GCG, glucagon; I.P., intraperitoneal.

pipette, which was then inserted through a trocar (Fig. 8I and fig. S18A). Under laparoscopic visualization, the device was implanted into the dog's peritoneal cavity by flushing the device with saline through the trocar (fig. S18B and movies S3). The device was implanted freely in the I.P. cavity without anchoring and placed in the cranial abdomen near the liver (Fig. 8J). Two weeks later, the device was retrieved by grasping one end of the device using laparoscopic forceps and pulling the device through a trocar (Fig. 8K). In two dogs, minor adhesions occurred between the peritoneal wall and a short segment of the device. In another dog, there was a point adhesion to the liver. In all three dogs, adhesions were considered minor and easy to separate, and the devices were all retrievable in their entirety (Fig. 8L, fig. S18C, and movies S4 and S5). The SC-β cells were still encapsulated in intact alginate hydrogel within retrieved

devices (Fig. 8M). In addition, although many cells were dead (fig. S18D), likely due to the severe immune responses in the challenging xenogeneic setting, it was unexpected to observe viable cells through live/dead staining (Fig. 8N). The H&E staining and immunofluorescent staining of insulin and glucagon also confirmed the viability and function of some cells (Fig. 8, O and P). These stringent, exploratory studies in immunocompetent mice and dogs, which may be more immunologically challenging than the scenario of human trial, demonstrated the feasibility of the NICE device for SC-β cell delivery from a procedural perspective.

DISCUSSION

In this study, we developed a nanofibrous-skin, hydrogel-core encapsulation device for the safe delivery of insulin-producing cells, especially human SC-β cells. The design takes advantage of the unique, tunable nanofibrous structure of electrospun nonwoven membranes and the biocompatible, tough, and easy-to-process TSPU polymer. With proper nanofiber size (<500 nm) and membrane thickness (~100 μm), the nanofibrous skin prevented cell escape or penetration while maintaining superb mass transfer. Inside the device, we used a common, easy–to–cross-link alginate hydrogel to disperse the islets and avoid cell clumping for better access to nutrients, notably oxygen (*38*). In addition, alginate hydrogel materials are immunoprotective (*39*), support the survival of islets via high hydration (*40*), and reduce diffusion of some antibodies (*41*). The whole device is soft but tough, easy to fabricate, and does not require any extra internal or external support to maintain its shape, leaving a unique nanofibrous surface as the host interface.

The long-term efficacy of cell encapsulation devices is highly dependent on the biocompatibility of the material and the transplantation site. We explored three clinically relevant transplant sites for the NICE device: the I.P. space, the E.F.P. (*42*), and the S.C. space (*43*). S.C. implantation was the least invasive transplantation site but caused the thickest FBR-induced fibrotic deposition around the device; modification of the site to induce a supporting vasculature will likely be needed for future development (*31*, *44*–*47*). Implantation in the E.F.P. (as a surrogate for the omentum) would provide access to vasculature (*48*), but the device-tissue adhesion observed during retrieval may become a challenge for clinical applications. On the other hand, the I.P. space was accessible, allowed facile retrieval of the device without severe adhesion, and caused the least cellular overgrowth. We attribute the minimal fibrotic reaction against the NICE device to both the biocompatibility of the TSPU polymer and the softness and nanofibrous structures of the electrospun nanomembranes. Previous studies have demonstrated that nanofibers may more closely mimic the natural extracellular matrix compared to microfibers and provide unique contact cues to modulate macrophages toward anti-inflammatory phenotypes in vitro and in vivo (*49*, *50*).

In addition to good biocompatibility, the function of the islets in the encapsulation device also highly depends on mass transfer. Pores should be sufficiently small to prevent direct contact between the host immune cells and the encapsulated cells. It is difficult to measure the precise pore sizes of an electrospun nonwoven membrane; however, the average pore size for the NICE device was estimated to be about 1 μm, which was effective in preventing the invasion of immune cells into the device in most cases, perhaps also partly due to the nonwoven, multilayer nature of the membrane. Research has been directed at modifying the structure of electrospun membranes to increase cell infiltration when that is desirable (*51*). Note that the range of pore sizes for the NICE device is much larger than pores in other previously reported devices, which are on the order of 10 to 100 nm. The relatively large pore size allows better mass transfer of nutrients, insulin, and metabolic wastes. Also note that the alginate hydrogel core of the device likely played a role in the immunoprotection. Our results with proliferative cells confirmed that the NICE device was both safe and functional, preventing cell infiltration or escape while maintaining cell viability for 5 months.

In addition to a feasible implantation site and a safe and functional device, islet source is another factor that determines the clinical success of a cell replacement therapy. Thus, in this study, we established the performance of our device using multiple islet sources to mimic different clinical scenarios. Currently, both islet autotransplantation after total pancreatectomy for the indication of pancreatitis and allotransplantation with immunosuppression for the treatment of T1D have been demonstrated to be clinically feasible (*52*, *53*). We showed that the NICE device protected syngeneic and allogeneic islets to correct diabetes in immunocompetent mice for up to 200 days. Although we achieved promising results with these cell sources, the search for a more ideal cell source continues. There is much research interest in xenotransplantation of porcine islets, due to donor tissue abundance, economic considerations (*39*, *54*, *55*), and, in particular, the recent advancement of genome editing to inactivate the porcine endogenous retrovirus (*56*). However, it is likely challenging for devices alone, without any immunosuppression, to protect and support the function of porcine islets in humans. Comparisons of diabetes correction results in mice using rat islets to that using mouse islets, or the functional outcome of human SC-β cells implanted in immunodeficient mice to that in immunocompetent ones, suggest that the NICE device will be better suited for allogeneic than xenogeneic transplantation.

To better understand the immunoprotective function of the device with the different islet sources, we examined the composition of the cells surrounding the device after transplantation and the antibody concentrations in circulation, in the I.P. fluid surrounding the device, and within the device. Different types of immune cells surrounded the device, including $CD4^+$ T cells, B cells, macrophages, dendritic cells, and neutrophils; however, very few $CD8^+$ T cells were present even in xenografts. This may be important because $CD8^+$ T cells are known to be recruited in nonimmunoprotected β cell transplantation and can directly destroy allogeneic islets by releasing granzyme B and perforins (*28*, *57*). Moreover, antibody analysis showed that there were elevated IgG and IgM concentrations and existence of alloantibodies in the serum of recipient mice and that a stronger antibody response was found in the mice with devices encapsulating xenogeneic islets than in those with devices encapsulating syngeneic or allogeneic islets. The antibody response is not unexpected because the device can prevent direct immune recognition but small–molecular weight shed antigens can still diffuse out of the device and elicit immune responses by indirect recognition. However, results showed that almost no alloantibodies were present inside the device. This is likely because the nanofiber membrane and the alginate core combinedly present diffusion barriers for the relatively large antibodies. Last, we expect that small-molecule cytokines such as interferon-γ, interleukin-1β, and tumor necrosis factor–α, with molecular weights of 17 to 51 kDa and hydrodynamic radii of 2 to 3 nm, can likely diffuse into the device

and may cause harmful effects on islets over time (*28*, *58*, *59*). Delivery of anti-inflammatory agents has been demonstrated to reduce cytokine-induced islet death (*60*, *61*). Nevertheless, these immunological analyses confirm the immunoprotective function of the NICE device as supported by the functional data with multiple islet sources.

Human SC-β cells are one of the most promising alternative cell sources for diabetes cell replacement therapy. A critical challenge, however, is the delivery of these cells, ideally in a safe and retrievable device without immunosuppression. In particular, because the autoimmune disease process that originally destroyed β cells in the pancreas may be reinvigorated by the introduction of new insulin-producing cells (*62*), methods including development of safe encapsulation devices to prevent both allo- and autoimmunity without systemic immunosuppression are needed (*63*–*70*). We showed that the NICE device was effective in supporting the function of relatively mature human SC-β cells and reversing diabetes in both immunodeficient mice (for up to 120 days) and immunocompetent mice (for up to 60 days). It is also noted that diabetes correction occurred within a week after transplantation.

Limitations exist in this study. For example, early failures in engraftments were observed and might be due to factors including sealing defects (fig. S19A), material defects (fig. S19B), unintentional inconsistencies in encapsulation and surgical procedures, number and quality of islets, and biological variations of recipients. Quality control of cells and devices will be critical to minimizing early failures and to eventually making the cell encapsulation a clinical reality. More specifically, for our device, quality control strategies include standardizing the fabrication and examining representative devices from every batch, including scanning electron microscopy, tensile test, porosity measurement, in vitro biocompatibility with islets, and in vivo biocompatibility; only after passing these assessments could that batch of devices be used in islet and β cell encapsulation (fig. S20). Another limitation is the lack of ideal animal models used in our study. The true potential of the NICE device for human SC-β cell–based T1D therapy would be best tested in human patients in an allogeneic setting. As a preclinical proof of concept, we tested the scalability, safety, and procedural feasibility (i.e., handling, implantation, and retrieval) of the device with human SC-β cells in healthy dogs. Despite the challenging xenogeneic environment and use of a short, 2-week transplantation, we observed viable and functional SC-β cells in retrieved devices, and the device was safe, relatively easy to implant, and completely retrievable using minimally invasive laparoscopic procedures. Longer-term implantation will likely lead to more tissue adhesions, rendering retrieval less smooth. The fibrotic cellular overgrowth after long-term implantation in large-animal models or human patients is another major challenge for clinical applications. Given our mouse studies, which suggest that the NICE device supported long-term function of allogeneic cells even in presence of cellular overgrowth, it remains to be investigated what amount of fibrotic deposition may be permissible for cellular function in higher-order animals or human patients and whether additional fibrosis-mitigating coatings (*18*) may be applicable to improve device function.

In conclusion, rapid advances in stem cell technology in recent years (*6*–*10*) have fueled hope that SC-β cells may be used in patients with diabetes to functionally cure T1D. To enable these therapies, encapsulation represents a promising, immunosuppression-free method to protect the cells from the autoimmune and alloimmune attack while mitigating potential risks such as teratoma formation by undifferentiated stem cells (*22*). In this work, we report the NICE device as a translatable strategy in the delivery of insulin-producing cells, in particular human SC-β cells. The low complexity design, the relatively easy fabrication, and the balance of safety and function make the NICE device an ideal candidate for future development and eventual clinical applications.

MATERIALS AND METHODS

Study design

The purpose of this study was to design a scalable device to deliver insulin-producing cells, in particular human SC-β cells, for T1D treatment. Animals were handled and cared by trained scientists and approved by the Cornell Institutional Animal Care and Use Committee. We carried out islet encapsulation experiments using different types of islets in the I.P. space in mice to examine islet viability and function in this device and scaled up the device using human SC-β cells in healthy dogs to test its safety, retrievability, and biocompatibility. Rodent islets were transplanted in immunocompetent diabetic mouse models, human islets were transplanted into immunodeficient diabetic mouse models, and human SC-β cells were transplanted into immunodeficient and immunocompetent diabetic mouse models, as well as immunocompetent healthy dogs. The optimal number of islets used in each study was determined on the basis of previous experience. Sample size, including number of mice per group, was chosen to ensure adequate power and was based on historical data. All mice used were males to eliminate any potential confounding influences of gender differences. All mice were randomly assigned to treatment groups, and all analyses were performed blinded to treatment conditions. No animals were excluded from analysis, and no outliers were excluded. The number of biologic replicates is specified in the figure legends.

Chemicals

Calcium chloride ($CaCl_2$), barium chloride ($BaCl_2$), sodium chloride (NaCl), potassium chloride (KCl), tetrahydrofuran (THF), and *N*,*N*′-dimethylformamide (DMF) were purchased from Sigma-Aldrich Co. (St. Louis, MO). Glucose was purchased from Mallinckrodt Pharmaceuticals (Dublin, Ireland). Ultrapure, sterile sodium alginate (SLG100) was purchased from FMC BioPolymer Co. (Philadelphia, PA). TSPU, a product of DSM Biomedical (CarboSil, Exton, PA, USA), was received as a gift.

Animals

Eight-week-old male C57BL/6, BALB/c, friend virus B (FVB)–Tg(CAG-luc,-GFP)L2G85Chco/J (L2G85), and NSG mice were purchased from the Jackson laboratory (Bar Harbor, ME). SCID-beige mice were obtained from Taconic Farms (Hudson, NY). Sprague-Dawley rats were obtained from Charles River Laboratories (Wilmington, MA). Human islets were provided by Y. Wang from Division of Transplant Surgery, University of Virginia and C. Liu and A. Naji from Department of Surgery, Hospital of the University of Pennsylvania. Beagle dogs were obtained from Marshall BioResources (Clyde, NY). All animal procedures were approved by the Cornell Institutional Animal Care and Use Committee.

Stem cell differentiation

Viable HUES8 human embryonic stem cells (18×10^6) were seeded into a 30-ml spinner flask. The cells were cultured in mTeSR1 for

72 hours and then differentiation initiated. The table (table S1) detailed the duration, basal media, and added supplements for each stage of differentiation. On the first day of stage 6, the cells were resized by single-cell dispersion with TrypLE at 37°C. The cells were then replanted in S6 media, replenished every other day, and placed on an orbital shaker (Benchmark) set at 100 revolutions per minute (rpm) in six-well plates (*6*, *9*).

Flow cytometry

Clusters were single cell dispersed with TrypLE in a water bath at 37°C. The cells were washed with phosphate-buffered saline (PBS) once and then fixed with 4% paraformaldehyde overnight at 4°C. The cells were blocked with staining buffer [5% donkey serum (Jackson Immunoresearch, 017-000-121) and 0.1% Triton X-100 (Acros Organics, 327371000) in PBS)], incubated overnight at 4°C with primary antibodies (table S2), washed with staining buffer, stained with secondary antibodies (table S2) for 2 hours at room temperature, and resuspended in staining buffer to analyze on a LSR II (BD Biosciences). FlowJo was used to generate dot plots and percentages.

Device fabrication

Different concentrations [8, 10, 12, and 14% (w/v)] of TSPU solutions were prepared by dissolving TSPU in a mixture of THF and DMF (3:2). The custom-built electrospinning device was equipped with a syringe pump (Harvard Apparatus, MA), a 10-ml syringe, a stainless-steel blunt needle, a constantly moving needle holder, a rotating collector, and a high-voltage supply (Gamma High Voltage, Ormond Beach, FL). The nanofibers were spun at 13 kV with a pumping rate of 0.5 ml/hour and with a 23-gauge (G) blunt needle as the spinneret. The spinneret was mounted on a sliding table moving back and forth with a speed of 5 cm/s. Working distance was fixed at 10 cm. A rotating target (i.e., stainless-steel rods with diameters ranging from 0.5 to 3 mm) was placed in the path of the polymer solution jet. The rod was connected to a motor controlled by rheostat (VWR, PA) and rotated at 400 to 500 rpm. The rod template was precoated with a thin layer of sucrose. The nanofibrous tubes were removed from the template by soaking in water. The tubes were cut into desired length and sealed at one end by hand impulse sealer (Impulse Sealer Supply, CA). The devices were soaked in 70% ethanol and sterilized using ultraviolet light for further study.

Isolation of rodent pancreatic islets

Mouse pancreatic islets were isolated from 8-week-old male C57BL/6 mice, BALB/c mice, or L2G85 mice. For mice, one bottle of collagenase (CIzyme RI 005-1030; VitaCyte, Indiana, USA) was reconstituted in 30 ml of M199 media (Gibco, USA). The bile duct was cannulated with a 27-G needle as described previously (*71*), and the pancreas was distended with cold collagenase. The perfused pancreases were then removed and digested in a 37°C water bath for 17 min. Sprague-Dawley rats from Charles River Laboratories weighing about 300 g were used for harvesting islets. For rat islet isolation, one bottle of Liberase (Research Grade, Roche) was reconstituted in 33 ml of M199 media (Gibco, USA). Briefly, the bile duct was cannulated, and the pancreas was distended by an injection of Liberase solution. The pancreas was digested in a 37°C water bath for 28 min. The purification of rodent islets was detailed in the Supplementary Materials. Purified islets were hand-counted by aliquot under a stereomicroscope (Olympus, SZ61). Islets were then cultured in RPMI 1640 media with 10% fetal bovine serum (FBS) and 1% penicillin/streptomycin for further use.

Isolation of human pancreatic islets

The pancreatic organs were obtained from the organ procurement organization under the United Network for Organ Sharing. The islets were isolated in the Human Islet Core at the University of Pennsylvania following the guidelines of Clinical Islet Transplantation (CIT) consortium protocols (*72*). Briefly, the pancreas was digested after intraductal injection of collagenase and neutral protease enzyme in Hanks' balanced salt solution. Liberated islets were then purified on continuous density gradients (Cellgro/Mediatech) using the COBE 2991 centrifuge, cultured in CIT culture media, and kept in a humidified 5% CO_2 incubator.

Cell encapsulation for mouse study

For a typical mouse study, the electrospun nanofiber device with a diameter of 1 mm was cut into lengths of 2.5 cm. Immediately, before encapsulation, the cultured islets (300 to 350 IEQ) were centrifuged at 1000 rpm for 1 min and all supernatant was aspirated. Twenty microliters of 2% (w/v) solution of SLG100 alginate dissolved in 0.9% (w/v) NaCl solution was added into the islets pellet. The cell-loaded alginate solution was filled into the device. For human islets, ~800 IEQ were collected and loaded with alginate as described above. For SC-β cells, ~1250 clusters were used. The device was further submerged in a cross-linking buffer containing 100 mM $CaCl_2$ and 5 mM $BaCl_2$. The device was taken out and extra solution on the surface of the device was removed with autoclaved tissue. The end of the tube was thermally sealed with hand impulse sealer (Impulse Sealer Supply). The device was washed with 0.9% (w/v) NaCl solution and ready to use.

Bioluminescence imaging

The GFP/luciferase-expressing aggregates were collected and centrifuged at 1000 rpm for 3 min. The cells were washed with saline and centrifuged again to form a pellet. Then, 300 to 400 GFP/luciferase MSC or 4T1 spheroids were loaded with alginate into the NICE device as described above. The GFP/luciferase MSC- or 4T1-laden devices were implanted into healthy C57BL/6 mice. The GFP/luciferase islet–laden device was prepared as described above and implanted into healthy C57BL/6 mice. The mice were injected with luciferin (150 mg/kg body weight; PerkinElmer, no. 122799) and imaged with IVIS Spectrum System (PerkinElmer) at the Biotechnology Resource Center at Cornell.

Transplantation and retrieval of the device in mice

For diabetes study, immunocompetent male C57BL/6 or immunodeficient male SCID-beige or male NSG mice were used for transplantation. To create diabetic mice, mice were injected I.P. with freshly prepared STZ (130 mg/kg body weight; Sigma-Aldrich) solution (13 mg/ml in 5 mM sodium citrate buffer solution). Only mice whose nonfasted blood glucose concentrations were above 300 mg/dl with two consecutive measurements were considered diabetic and underwent transplantation. Detailed procedure of transplantation can be found in the Supplementary Materials. Glucose was monitored twice a week. A small drop of blood was collected from the tail vein using a lancet and tested using a commercial glucometer (CONTOUR NEXT, Ascensia Diabetes Care, NJ). Mice changing from a diabetic state (blood glucose greater than ~350 mg/dl for at

least two consecutive measurements) to a nondiabetic state (blood glucose less than ~200 mg/dl for at least two consecutive measurements) were considered as engrafted mice. For all the engrafted mice, devices were explanted in a survival surgery after a certain time, and the mice remained alive after retrieval. Blood glucose was monitored after explanting the device to further confirm the function of the device. Some retrieved samples were examined by ex vivo GSIS test (described in the Supplementary Materials) and fixed in 10% formalin for further staining. For the other devices, the nanofibrous skin was peeled off, and the islet-laden alginate inside the device was imaged using the stereomicroscope.

IPGTT

Mice were fasted overnight before receiving an I.P. glucose bolus (2 g/kg body weight). The healthy mice and diabetic mice were used as positive control and negative control, respectively. Blood glucose was monitored at regular intervals (time: 0, 5, 15, 30, 60, 90, and 120 min) after injection, allowing for the AUC to be calculated and analyzed between groups.

In vivo GSIS

The SCID-beige mice implanted with human islet–laden devices or NSG mice implanted with SC-β cells were fasted overnight before receiving an I.P. glucose bolus (2 g/kg body weight). Blood was collected from the orbital vein before injection and 90 min after injection using a tube with clotting activator (Microvette 300 Z, Sarstedt). The tubes were then centrifuged at 2000 relative centrifugal force (rcf) for 10 min. Serum was collected from the tube and frozen for further analysis. Human C-peptide concentration in the serum was detected using ultrasensitive human C-peptide enzyme-linked immunosorbent assay kit (Mercodia).

Cellular analysis of fibrotic layer by flow cytometry

After the engrafted devices were retrieved from the recipients, the fibrotic layer surrounding the encapsulation device was carefully peeled off using tweezers. The fibrotic layer was cut into small pieces and digested with type I collagenase (1 mg/ml; Worthington Biochemical Corporation, LS004194) for 1 hour in incubator. The digestion was stopped by adding cell culture medium containing 10% FBS. The cell solution was filtered through a Falcon 40-μm strainer (Corning, 431750) to get single-cell solution. Cells were centrifuged at 1000 rpm for 5 min. Supernatant was discarded, and cells were washed with PBS solution to remove the remaining FBS. The cells were stained with the Zombie Yellow Fixable Viability Kit (BioLegend, 423103) following the manufacturer's instructions. Cells were washed one time with 2 ml of Cell Staining Buffer (BioLegend, 420201) and centrifuged into a pellet. Fc receptors were blocked by preincubating cells with TruStain FcX PLUS (anti-mouse CD16/32) Antibody (BioLegend, 156603) in 100 μl of Cell Staining Buffer for 5 min on ice. Then, cells were labeled with mixed antibodies (table S3) on ice for 15 min. The cells were washed twice with 2 ml of Cell Staining Buffer by centrifugation at 350 rcf for 5 min. The cell pellet was resuspended in 0.5 ml of Cell Staining Buffer. UltraComp eBeads Compensation Beads (Thermo Fisher Scientific, 01-2222-41) incubated with each antibody following manufactures' instruction were used for compensation. Last, stained cells were analyzed using the Attune NxT Flow Cytometer (Thermo Fisher Scientific). The data were analyzed by FlowJo software v10.7.

Cell encapsulation for dog experiment

Three devices about 17 cm long were prepared and sterilized as mentioned above. A total of 2500 clusters of SC-β cells were suspended in 140 μl of 2% SLG100 solution and loaded into one device using PE50 tubing. The device was cross-linked and sealed as mentioned above. The devices were submerged in 0.9% saline and ready for implantation.

Laparoscopic implantation and retrieval in dogs

Dogs were premedicated with glycopyrrolate and butorphanol, induced with propofol, and anesthetized with isoflurane and oxygen. The abdomen was clipped and prepared for sterile surgery. A 10-mm laparoscopic camera port and two 5-mm instrument ports were percutaneously inserted into the abdomen. The abdomen was insufflated to 12-mmHg pressure with CO_2. The device in a 10-ml pipette was inserted into the abdomen through the left-sided instrument port. Then, the device was flushed out from the pipette using sterile saline. A laparoscopic probe was introduced through the right-sided 5-mm port and was used to manipulate the device so that it was placed between the liver and the diaphragm. The remaining ports were then removed, and the port sites were closed with 3-0 polydioxanone suture material. For retrieval of the devices, the procedure was similar using one 10-mm camera port and one or two 5-mm instrument ports. The previously implanted device was located and photographed. The device was grasped with laparoscopic Kelly forceps.

Histological analysis

The implants were harvested from the mice and fixed in 10% formalin, dehydrated with graded ethanol solutions, embedded in paraffin, and sectioned by Cornell Histology Core Facility. The samples were sliced on a microtome at a thickness of 5 μm. The sections were stained with H&E and then imaged by a microscope (IN200TC, AmScope). To conduct immunofluorescent staining, the histological slides were deparaffinized, followed by antigen retrieval as described before (*42*). Nonspecific binding was blocked via incubation with 5% donkey serum (S30-M; Sigma-Aldrich) for 1 hour at room temperature. Sections were decanted and incubated with primary antibodies overnight at 4°C. The sections were then washed and incubated with the fluorescence-conjugated secondary antibodies for 1 hour at room temperature. Nuclei were labeled with 4′,6-diamidino-2-phenylindole (DAPI), and slides were covered with fluorescent mounting medium (F6057; Sigma-Aldrich). Last, the sections were imaged through confocal microscopy (FV1000; Olympus, Japan). The antibodies used here were listed in table S4. The thickness of fibrotic layer, the density of αSMA^+ cells, and the percentage of hormone-expressing cells were analyzed using ImageJ software. More experimental methods were detailed in the Supplementary Materials.

Statistical analysis

Unless otherwise stated, data were expressed as means ± SD. For comparisons between two groups, means were compared using two-tailed Student's *t* tests. Comparisons between multiple groups were performed by analysis of variance (ANOVA) followed by Tukey's post hoc analysis. Sample size, including number of mice per group, was chosen to ensure adequate power and was based on historical data. No exclusion criteria were applied for all analyses. All statistical analyses were performed using GraphPad Prism v.8

software (GraphPad Software Inc.). The level of significance was assessed starting at $P < 0.05$.

SUPPLEMENTARY MATERIALS

stm.sciencemag.org/cgi/content/full/13/596/eabb4601/DC1
Materials and Methods
Figs. S1 to S20
Tables S1 to S4
Movies S1 to S5

View/request a protocol for this paper from *Bio-protocol*.

REFERENCES AND NOTES

1. E. Latres, D. A. Finan, J. L. Greenstein, A. Kowalski, T. J. Kieffer, Navigating two roads to glucose normalization in diabetes: Automated insulin delivery devices and cell therapy. *Cell Metab.* **29**, 545–563 (2019).
2. C. Aguayo-Mazzucato, S. Bonner-Weir, Pancreatic β cell regeneration as a possible therapy for diabetes. *Cell Metab.* **27**, 57–67 (2018).
3. A. M. J. Shapiro, C. Ricordi, B. J. Hering, H. Auchincloss, R. Lindblad, R. P. Robertson, A. Secchi, M. D. Brendel, T. Berney, D. C. Brennan, E. Cagliero, R. Alejandro, E. A. Ryan, B. DiMercurio, P. Morel, K. S. Polonsky, J.-A. Reems, R. G. Bretzel, F. Bertuzzi, T. Froud, R. Kandaswamy, D. E. R. Sutherland, G. Eisenbarth, M. Segal, J. Preiksaitis, G. S. Korbutt, F. B. Barton, L. Viviano, V. Seyfert-Margolis, J. Bluestone, J. R. T. Lakey, International trial of the Edmonton protocol for islet transplantation. *N. Engl. J. Med.* **355**, 1318–1330 (2006).
4. A. M. J. Shapiro, J. R. T. Lakey, E. A. Ryan, G. S. Korbutt, E. Toth, G. L. Warnock, N. M. Kneteman, R. V. Rajotte, Islet transplantation in seven patients with type 1 diabetes mellitus using a glucocorticoid-free immunosuppressive regimen. *N. Engl. J. Med.* **343**, 230–238 (2000).
5. B. J. Hering, W. R. Clarke, N. D. Bridges, T. L. Eggerman, R. Alejandro, M. D. Bellin, K. Chaloner, C. W. Czarniecki, J. S. Goldstein, L. G. Hunsicker, D. B. Kaufman, O. Korsgren, C. P. Larsen, X. Luo, J. F. Markmann, A. Naji, J. Oberholzer, A. M. Posselt, M. R. Rickels, C. Ricordi, M. A. Robien, P. A. Senior, A. M. J. Shapiro, P. G. Stock, N. A. Turgeon; Clinical Islet Transplantation Consortium, Phase 3 trial of transplantation of human islets in type 1 diabetes complicated by severe hypoglycemia. *Diabetes Care* **39**, 1230–1240 (2016).
6. F. W. Pagliuca, J. R. Millman, M. Gürtler, M. Segel, A. Van Dervort, J. H. Ryu, Q. P. Peterson, D. Greiner, D. A. Melton, Generation of functional human pancreatic β cells in vitro. *Cell* **159**, 428–439 (2014).
7. A. Rezania, J. E. Bruin, P. Arora, A. Rubin, I. Batushansky, A. Asadi, S. O'Dwyer, N. Quiskamp, M. Mojibian, T. Albrecht, Y. H. C. Yang, J. D. Johnson, T. J. Kieffer, Reversal of diabetes with insulin-producing cells derived in vitro from human pluripotent stem cells. *Nat. Biotechnol.* **32**, 1121–1133 (2014).
8. J. R. Millman, C. Xie, A. V. Dervort, M. Gürtler, F. W. Pagliuca, D. A. Melton, Generation of stem cell-derived β-cells from patients with type 1 diabetes. *Nat. Commun.* **7**, 11463 (2016).
9. L. Velazco-Cruz, J. Song, K. G. Maxwell, M. M. Goedegebuure, P. Augsornworawat, N. J. Hogrebe, J. R. Millman, Acquisition of dynamic function in human stem cell-derived β cells. *Stem Cell Rep.* **12**, 351–365 (2019).
10. G. G. Nair, J. S. Liu, H. A. Russ, S. Tran, M. S. Saxton, R. Chen, C. Juang, M. Li, V. Q. Nguyen, S. Giacometti, S. Puri, Y. Xing, Y. Wang, G. L. Szot, J. Oberholzer, A. Bhushan, M. Hebrok, Recapitulating endocrine cell clustering in culture promotes maturation of human stem-cell-derived β cells. *Nat. Cell Biol.* **21**, 263–274 (2019).
11. K. G. Maxwell, P. Augsornworawat, L. Velazco-Cruz, M. H. Kim, R. Asada, N. J. Hogrebe, S. Morikawa, F. Urano, J. R. Millman, Gene-edited human stem cell–derived β cells from a patient with monogenic diabetes reverse preexisting diabetes in mice. *Sci. Transl. Med.* **12**, eaax9106 (2020).
12. G. C. Weir, B.-W. Susan, Scientific and political impediments to successful islet transplantation. *Diabetes* **46**, 1247–1256 (1997).
13. E. Zahr, R. D. Molano, A. Pileggi, H. Ichii, S. S. Jose, N. Bocca, W. An, J. Gonzalez-Quintana, C. Fraker, C. Ricordi, L. Inverardi, Rapamycin impairs in vivo proliferation of islet beta-cells. *Transplantation* **84**, 1576–1583 (2007).
14. H. Hentze, P. L. Soong, S. T. Wang, B. W. Phillips, T. C. Putti, N. R. Dunn, Teratoma formation by human embryonic stem cells: Evaluation of essential parameters for future safety studies. *Stem Cell Res.* **2**, 198–210 (2009).
15. O. Veiseh, J. C. Doloff, M. Ma, A. J. Vegas, H. H. Tam, A. R. Bader, J. Li, E. Langan, J. Wyckoff, W. S. Loo, S. Jhunjhunwala, A. Chiu, S. Siebert, K. Tang, J. Hollister-Lock, S. Aresta-Dasilva, M. Bochenek, J. Mendoza-Elias, Y. Wang, M. Qi, D. M. Lavin, M. Chen, N. Dholakia, R. Thakrar, I. Lacík, G. C. Weir, J. Oberholzer, D. L. Greiner, R. Langer, D. G. Anderson, Size- and shape-dependent foreign body immune response to materials implanted in rodents and non-human primates. *Nat. Mater.* **14**, 643–651 (2015).
16. T. Wang, I. Lacík, M. Brissová, A. V. Anilkumar, A. Prokop, D. Hunkeler, R. Green, K. Shahrokhi, A. C. Powers, An encapsulation system for the immunoisolation of pancreatic islets. *Nat. Biotechnol.* **15**, 358–362 (1997).
17. A. J. Vegas, O. Veiseh, J. C. Doloff, M. Ma, H. H. Tam, K. Bratlie, J. Li, A. R. Bader, E. Langan, K. Olejnik, P. Fenton, J. W. Kang, J. Hollister-Locke, M. A. Bochenek, A. Chiu, S. Siebert, K. Tang, S. Jhunjhunwala, S. Aresta-Dasilva, N. Dholakia, R. Thakrar, T. Vietti, M. Chen, J. Cohen, K. Siniakowicz, M. Qi, J. McGarrigle, A. C. Graham, S. Lyle, D. M. Harlan, D. L. Greiner, J. Oberholzer, G. C. Weir, R. Langer, D. G. Anderson, Combinatorial hydrogel library enables identification of materials that mitigate the foreign body response in primates. *Nat. Biotechnol.* **34**, 345–352 (2016).
18. N. Bray, Biomaterials: Modified alginates provide a long-term disguise against the foreign body response. *Nat. Rev. Drug Discov.* **15**, 158 (2016).
19. Q. Liu, A. Chiu, L.-H. Wang, D. An, M. Zhong, A. M. Smink, B. J. de Haan, P. de Vos, K. Keane, A. Vegge, E. Y. Chen, W. Song, W. F. Liu, J. Flanders, C. Rescan, L. G. Grunnet, X. Wang, M. Ma, Zwitterionically modified alginates mitigate cellular overgrowth for cell encapsulation. *Nat. Commun.* **10**, 5262 (2019).
20. A. J. Vegas, O. Veiseh, M. Gürtler, J. R. Millman, F. W. Pagliuca, A. R. Bader, J. C. Doloff, J. Li, M. Chen, K. Olejnik, H. H. Tam, S. Jhunjhunwala, E. Langan, S. Aresta-Dasilva, S. Gandham, J. J. McGarrigle, M. A. Bochenek, J. Hollister-Lock, J. Oberholzer, D. L. Greiner, G. C. Weir, D. A. Melton, R. Langer, D. G. Anderson, Long-term glycemic control using polymer-encapsulated human stem cell-derived beta cells in immune-competent mice. *Nat. Med.* **22**, 306–311 (2016).
21. D. A. Alagpulinsa, J. J. L. Cao, R. K. Driscoll, R. F. Sîrbulescu, M. F. E. Penson, M. Sremac, E. N. Engquist, T. A. Brauns, J. F. Markmann, D. A. Melton, M. C. Poznansky, Alginate-microencapsulation of human stem cell-derived β cells with CXCL12 prolongs their survival and function in immunocompetent mice without systemic immunosuppression. *Am. J. Transplant.* **19**, 1930–1940 (2019).
22. D. An, A. Chiu, J. A. Flanders, W. Song, D. Shou, Y.-C. Lu, L. G. Grunnet, L. Winkel, C. Ingvorsen, N. S. Christophersen, J. J. Fels, F. W. Sand, Y. Ji, L. Qi, Y. Pardo, D. Luo, M. Silberstein, J. Fan, M. Ma, Designing a retrievable and scalable cell encapsulation device for potential treatment of type 1 diabetes. *Proc. Natl. Acad. Sci. U.S.A.* **115**, E263–E272 (2018).
23. C. Haller, J. Piccand, F. D. Franceschi, Y. Ohi, A. Bhoumik, C. Boss, U. D. Marchi, G. Jacot, S. Metairon, P. Descombes, A. Wiederkehr, A. Palini, N. Bouche, P. Steiner, O. G. Kelly, M. R.-C. Kraus, Macroencapsulated human iPSC-derived pancreatic progenitors protect against STZ-induced hyperglycemia in mice. *Stem Cell Reports* **12**, 787–800 (2019).
24. M. Kumagai-Braesch, S. Jacobson, H. Mori, X. Jia, T. Takahashi, A. Wernerson, F.-T. Malin, A. Tibell, The TheraCyte™ device protects against islet allograft rejection in immunized hosts. *Cell Transplant.* **22**, 1137–1146 (2013).
25. J. E. Bruin, A. Rezania, J. Xu, K. Narayan, J. K. Fox, J. J. O'Neil, T. J. Kieffer, Maturation and function of human embryonic stem cell-derived pancreatic progenitors in macroencapsulation devices following transplant into mice. *Diabetologia* **56**, 1987–1998 (2013).
26. T. Robert, I. D. Mesmaeker, G. M. Stangé, K. G. Suenens, Z. Ling, E. J. Kroon, D. G. Pipeleers, Functional beta cell mass from device-encapsulated hESC-derived pancreatic endoderm achieving metabolic control. *Stem Cell Rep.* **10**, 739–750 (2018).
27. A. Rezania, J. E. Bruin, J. Xu, K. Narayan, J. K. Fox, J. J. O'Neil, T. J. Kieffer, Enrichment of human embryonic stem cell-derived NKX6.1-expressing pancreatic progenitor cells accelerates the maturation of insulin-secreting cells in vivo. *Stem Cells* **31**, 2432–2442 (2013).
28. G. Faleo, K. Lee, V. Nguyen, Q. Tang, Assessment of immune isolation of allogeneic mouse pancreatic progenitor cells by a macroencapsulation device. *Transplantation* **100**, 1211–1218 (2016).
29. R. Chang, G. Faleo, H. A. Russ, A. V. Parent, S. K. Elledge, D. A. Bernards, J. L. Allen, K. Villanueva, M. Hebrok, Q. Tang, T. A. Desai, Nanoporous immunoprotective device for stem-cell-derived β-cell replacement therapy. *ACS Nano* **11**, 7747–7757 (2017).
30. C. E. Nyitray, R. Chang, G. Faleo, K. D. Lance, D. A. Bernards, Q. Tang, T. A. Desai, Polycaprolactone thin-film micro- and nanoporous cell-encapsulation devices. *ACS Nano* **9**, 5675–5682 (2015).
31. A. R. Pepper, B. Gala-Lopez, R. Pawlick, S. Merani, T. Kin, A. M. J. Shapiro, A prevascularized subcutaneous device-less site for islet and cellular transplantation. *Nat. Biotechnol.* **33**, 518–523 (2015).
32. J. E. Mooney, B. E. Rolfe, G. W. Osborne, D. P. Sester, N. van Rooijen, G. R. Campbell, D. A. Hume, J. H. Campbell, Cellular plasticity of inflammatory myeloid cells in the peritoneal foreign body response. *Am. J. Pathol.* **176**, 369–380 (2010).
33. J. H. Campbell, J. L. Efendy, C.-L. Han, A. A. Girjes, G. R. Campbell, Haemopoietic origin of myofibroblasts formed in the peritoneal cavity in response to a foreign body. *J. Vasc. Res.* **37**, 364–371 (2000).
34. P.-O. Carlsson, F. Palm, A. Andersson, P. Liss, Markedly decreased oxygen tension in transplanted rat pancreatic islets irrespective of the implantation site. *Diabetes* **50**, 489–495 (2001).

35. H. Komatsu, F. Kandeel, Y. Mullen, Impact of oxygen on pancreatic islet survival. *Pancreas* **47**, 533–543 (2018).
36. R. Rodriguez-Diaz, R. D. Molano, J. R. Weitz, M. H. Abdulreda, D. M. Berman, B. Leibiger, I. B. Leibiger, N. S. Kenyon, C. Ricordi, A. Pileggi, A. Caicedo, P.-O. Berggren, Paracrine interactions within the pancreatic islet determine the glycemic set point. *Cell Metab.* **27**, 549–558.e4 (2018).
37. B. Svendsen, O. Larsen, M. B. N. Gabe, C. B. Christiansen, M. M. Rosenkilde, D. J. Drucker, J. J. Holst, Insulin secretion depends on intra-islet glucagon signaling. *Cell Rep.* **25**, 1127–1134.e2 (2018).
38. K. K. Papas, H. De Leon, T. M. Suszynski, R. C. Johnson, Oxygenation strategies for encapsulated islet and beta cell transplants. *Adv. Drug. Deliv. Rev.* **139**, 139–156 (2019).
39. A. Omer, V. F. Duvivier-Kali, N. Trivedi, K. Wilmot, S. Bonner-Weir, G. C. Weir, Survival and maturation of microencapsulated porcine neonatal pancreatic cell clusters transplanted into immunocompetent diabetic mice. *Diabetes* **52**, 69–75 (2003).
40. A. S. Hoffman, Hydrogels for biomedical applications. *Adv. Drug Deliv. Rev.* **64**, 3–23 (2012).
41. G. A. P. Juárez, M. Spasojevic, M. M. Faas, P. de Vos, Immunological and technical considerations in application of alginate-based microencapsulation systems. *Front. Bioeng. Biotechnol.* **2**, 26 (2014).
42. X. Wang, K. Wang, W. Zhang, M. Qiang, Y. Luo, A bilaminated decellularized scaffold for islet transplantation: Structure, properties and functions in diabetic mice. *Biomaterials* **138**, 80–90 (2017).
43. S. Merani, C. Toso, J. Emamaullee, A. M. J. Shapiro, Optimal implantation site for pancreatic islet transplantation. *Brit. J. Surg.* **95**, 1449–1461 (2008).
44. A. R. Pepper, R. Pawlick, A. Bruni, J. Wink, Y. Rafiei, D. O'Gorman, R. Yan-Do, B. Gala-Lopez, T. Kin, P. E. MacDonald, A. M. J. Shapiro, Transplantation of human pancreatic endoderm cells reverses diabetes post transplantation in a prevascularized subcutaneous site. *Stem Cell Rep.* **8**, 1689–1700 (2017).
45. W. Song, A. Chiu, L.-H. Wang, R. E. Schwartz, B. Li, N. Bouklas, D. T. Bowers, D. An, S. H. Cheong, J. A. Flanders, Y. Pardo, Q. Liu, X. Wang, V. K. Lee, G. Dai, M. Ma, Engineering transferrable microvascular meshes for subcutaneous islet transplantation. *Nat. Commun.* **10**, 4602 (2019).
46. D. T. Bowers, W. Song, L.-H. Wang, M. Ma, Engineering the vasculature for islet transplantation. *Acta Biomater.* **95**, 131–151 (2019).
47. A. E. Vlahos, N. Cober, M. V. Sefton, Modular tissue engineering for the vascularization of subcutaneously transplanted pancreatic islets. *Proc. Natl. Acad. Sci. U.S.A.* **114**, 9337–9342 (2017).
48. J. D. Weaver, D. M. Headen, J. Aquart, C. T. Johnson, L. D. Shea, H. Shirwan, A. J. García, Vasculogenic hydrogel enhances islet survival, engraftment, and function in leading extrahepatic sites. *Sci. Adv.* **3**, e1700184 (2017).
49. K. Garg, N. A. Pullen, C. A. Oskeritzian, J. J. Ryan, G. L. Bowlin, Macrophage functional polarization (M1/M2) in response to varying fiber and pore dimensions of electrospun scaffolds. *Biomaterials* **34**, 4439–4451 (2013).
50. K. Wang, W.-D. Hou, X. Wang, C. Han, I. Vuletic, N. Su, W.-X. Zhang, Q.-S. Ren, L. Chen, Y. Luo, Overcoming foreign-body reaction through nanotopography: Biocompatibility and immunoisolation properties of a nanofibrous membrane. *Biomaterials* **102**, 249–258 (2016).
51. S. Chen, H. Wang, A. McCarthy, Z. Yan, H. J. Kim, M. A. Carlson, Y. Xia, J. Xie, Three-dimensional objects consisting of hierarchically assembled nanofibers with controlled alignments for regenerative medicine. *Nano Lett.* **19**, 2059–2065 (2019).
52. R. P. Robertson, K. J. Lanz, D. E. R. Sutherland, D. M. Kendall, Prevention of diabetes for up to 13 years by autoislet transplantation after pancreatectomy for chronic pancreatitis. *Diabetes* **50**, 47–50 (2001).
53. J. R. Millman, F. W. Pagliuca, Autologous pluripotent stem cell–derived β-like cells for diabetes cellular therapy. *Diabetes* **66**, 1111–1120 (2017).
54. R. Krishnan, R. P. Arora, M. Alexander, S. M. White, M. W. Lamb, C. E. Foster III, B. Choi, J. R. T. Lakey, Noninvasive evaluation of the vascular response to transplantation of alginate encapsulated islets using the dorsal skin-fold model. *Biomaterials* **35**, 891–898 (2014).
55. I. D. Mesmaeker, T. Robert, K. G. Suenens, G. M. Stangé, F. V. Hulle, Z. Ling, P. Tomme, D. Jacobs-Tulleneers-Thevissen, B. Keymeulen, D. G. Pipeleers, Increase functional β-cell mass in subcutaneous alginate capsules with porcine prenatal islet cells but loss with human adult islet cells. *Diabetes* **67**, 2640–2649 (2018).
56. D. Niu, H.-J. Wei, L. Lin, H. George, T. Wang, I.-H. Lee, H.-Y. Zhao, Y. Wang, Y. Kan, E. Shrock, E. Lesha, G. Wang, Y. Luo, Y. Qing, D. Jiao, H. Zhao, X. Zhou, S. Wang, H. Wei, M. Güell, G. M. Church, L. Yang, Inactivation of porcine endogenous retrovirus in pigs using CRISPR-Cas9. *Science* **357**, 1303–1307 (2017).
57. S. J. F. Harper, J. M. Ali, E. Wlodek, M. C. Negus, I. G. Harper, M. Chhabra, M. S. Qureshi, M. Mallik, E. Bolton, J. A. Bradley, G. J. Pettigrew, CD8 T-cell recognition of acquired alloantigen promotes acute allograft rejection. *Proc. Natl. Acad. Sci. U.S.A.* **112**, 12788–12793 (2015).
58. M. C. Åkerfeldt, J. Howes, J. Y. Chan, V. A. Stevens, N. Boubenna, H. M. McGuire, C. King, T. J. Biden, D. R. Laybutt, Cytokine-induced β-cell death is independent of endoplasmic reticulum stress signaling. *Diabetes* **57**, 3034–3044 (2008).
59. G. Soldevila, M. Buscema, M. Doshi, R. F. L. James, G. F. Bottazzo, R. Pujol-Borrell, Cytotoxic effect of IFN-γ plus TNF-α on human islet cells. *J. Autoimmun.* **4**, 291–306 (1991).
60. K. Jiang, J. D. Weaver, Y. Li, X. Chen, J. Liang, C. L. Stabler, Local release of dexamethasone from macroporous scaffolds accelerates islet transplant engraftment by promotion of anti-inflammatory M2 macrophages. *Biomaterials* **114**, 71–81 (2017).
61. T. T. Dang, A. V. Thai, J. Cohen, J. E. Slosberg, K. Siniakowicz, J. C. Doloff, M. Ma, J. Hollister-Lock, K. M. Tang, Z. Gu, H. Cheng, G. C. Weir, R. Langer, D. G. Anderson, Enhanced function of immuno-isolated islets in diabetes therapy by co-encapsulation with an anti-inflammatory drug. *Biomaterials* **34**, 5792–5801 (2013).
62. L. Wen, R. E. Ley, P. Y. Volchkov, P. B. Stranges, L. Avanesyan, A. C. Stonebraker, C. Hu, F. S. Wong, G. L. Szot, J. A. Bluestone, J. I. Gordon, A. V. Chervonsky, Innate immunity and intestinal microbiota in the development of type 1 diabetes. *Nature* **455**, 1109–1113 (2008).
63. A. U. Ernst, L.-H. Wang, M. Ma, Islet encapsulation. *J. Mater. Chem. B* **6**, 6705–6722 (2018).
64. T. Desai, L. D. Shea, Advances in islet encapsulation technologies. *Nat. Rev. Drug Discov.* **16**, 338–350 (2017).
65. E. Dolgin, Diabetes: Encapsulating the problem. *Nature* **540**, S60–S62 (2016).
66. E. Dolgin, Encapsulate this. *Nat. Med.* **20**, 9–11 (2014).
67. G. Orive, D. Emerich, P. D. Vos, Reply to encapsulate this: The do's and don'ts. *Nat. Med.* **20**, 233 (2014).
68. S. Fuchs, A. U. Ernst, L.-H. Wang, K. Shariati, X. Wang, Q. Liu, M. Ma, Hydrogels in emerging technologies for type 1 diabetes. *Chem. Rev.* 10.1021/acs.chemrev.0c0106 (2020).
69. A. U. Ernst, D. T. Bowers, L.-H. Wang, K. Shariati, M. D. Plesser, N. K. Brown, T. Mehrabyan, M. Ma, Nanotechnology in cell replacement therapies for type 1 diabetes. *Adv. Drug Deliv. Rev.* **139**, 116–138 (2019).
70. T. A. Desai, Q. Tang, Islet encapsulation therapy—Racing towards the finish line? *Nat. Rev. Endocrinol.* **14**, 630–632 (2018).
71. K. Wang, X. Wang, C.-S. Han, L. Chen, Y. Luo, Scaffold-supported transplantation of islets in the epididymal fat pad of diabetic mice. *J. Vis. Exp.* **125**, 54995 (2017).
72. C. Ricordi, J. S. Goldstein, A. N. Balamurugan, G. L. Szot, T. Kin, C. Liu, C. W. Czarniecki, B. Barbaro, N. D. Bridges, J. Cano, W. R. Clarke, T. L. Eggerman, L. G. Hunsicker, D. B. Kaufman, A. Khan, D.-E. Lafontant, E. Linetsky, X. Luo, J. F. Markmann, A. Naji, O. Korsgren, J. Oberholzer, N. A. Turgeon, D. Brandhorst, X. Chen, A. S. Friberg, J. Lei, L. Wang, J. J. Wilhelm, J. Willits, X. Zhang, B. J. Hering, A. M. Posselt, P. G. Stock, A. M. J. Shapiro, X. Chen, National Institutes of Health–sponsored clinical islet transplantation consortium phase 3 trial: Manufacture of a complex cellular product at eight processing facilities. *Diabetes* **65**, 3418–3428 (2016).

Acknowledgments: We thank A. Chiu (Cornell University) for helping with the rat islet isolation. We thank N. Bouklas (Cornell University) for the discussions on the mechanical properties of the device. We thank Cornell Center for Materials Research Facility for the SEM images, which is supported by the NSF under award number DMR-1719875. We thank Cornell Histology Core Facility for the histological cross sectioning and staining. We thank S. Li (University of California, Los Angeles) for providing the polymer. We thank K. D'Amour (ViaCyte Inc.) for the MAFA antibody. We thank Y. Wang (University of Virginia), C. Liu, and A. Naji (Hospital of the University of Pennsylvania) for providing the human islets. **Funding:** This work was mainly sponsored by the Novo Nordisk Company and partially supported by the Juvenile Diabetes Research Foundation (JDRF, 2-SRA-2018-472-S-B), the Hartwell Foundation, and the NIH (1R01DK105967-01A1). J.R.M. was supported by the NIH (5R01DK114233) and JDRF (5-CDA-2017-391-A-N). K.G.M. was supported by the NIH (T32DK108742). The NIDDK IIDP (Integrated Islet Distribution Program) for the grant (Beckman Research Center, no. 10028044) was awarded to A.N. **Author contributions:** X.W. and M.M. conceived and designed the project. K.G.M. differentiated the cells and performed the in vitro and ex vivo analysis of SC-β cells. X.W. performed all the other in vitro analysis. X.W. and K.W. generated the GFP/luciferase-expressing cell lines and conducted the immunofluorescent staining. X.W. performed the in vivo studies. J.A.F., X.W., and Q.L. conducted the dog experiment. W.L. built the electrospinning system. X.W. and L.-H.W. drew the schematics. K.G.M. and J.R.M. provided the SC-β cells. C.L., A.N., and Y.W. provided the human islets. B.W. designed the flow cytometry antibody panel to analyze the immune cell populations deposited on the device. X.W., D.T.B., and M.M. wrote the manuscript. J.C., A.U.E., and J.M.M.-M. discussed the data and revised the manuscript. All authors edited and reviewed the manuscript. **Competing interests:** X.W., Q.L, J.A.F., and M.M. are inventors on a patent application (PCT/US2020/30798) submitted by

Cornell University that covers the device described in this manuscript. M.M. is a consultant for Ambys Medicines. M.M. is a scientific advisor for Beemmunity Inc. and a cofounder for Halomine Inc., both of which are unrelated to this paper. J.R.M. is an inventor on patents (10,030,229 and 10,190,096) held by the Harvard University and patent applications (PCT/US2019/032643 and PCT/US2020/061572) held by the Washington University that cover the SC-β cell technology described in this manuscript. J.R.M. is a consultant for Sana Biotechnology. K.G.M. is the Chief Operations Officer and cofounder of Salentra Biosciences. J.R.M. is the Chief Scientific Officer and cofounder of Salentra Biosciences. The other authors declare that they have no competing interests. **Data and materials availability:** All data associated with this study are presented in the paper and/or the Supplementary Materials.

Submitted 26 February 2020
Resubmitted 9 February 2021
Accepted 28 April 2021
Published 2 June 2021
10.1126/scitranslmed.abb4601

Citation: X. Wang, K. G. Maxwell, K. Wang, D. T. Bowers, J. A. Flanders, W. Liu, L.-H. Wang, Q. Liu, C. Liu, A. Naji, Y. Wang, B. Wang, J. Chen, A. U. Ernst, J. M. Melero-Martin, J. R. Millman, M. Ma, A nanofibrous encapsulation device for safe delivery of insulin-producing cells to treat type 1 diabetes. *Sci. Transl. Med.* **13**, eabb4601 (2021).

Science Translational Medicine

A nanofibrous encapsulation device for safe delivery of insulin-producing cells to treat type 1 diabetes

Xi WangKristina G. MaxwellKai WangDaniel T. BowersJames A. FlandersWanjun LiuLong-Hai WangQingsheng LiuChengyang LiuAli NajiYong WangBo WangJing ChenAlexander U. ErnstJuan M. Melero-MartinJeffrey R. MillmanMinglin Ma

Sci. Transl. Med., 13 (596), eabb4601. • DOI: 10.1126/scitranslmed.abb4601

Capitalizing on encapsulation

Encapsulating pancreatic islets or # cells before transplant is a promising approach for type 1 diabetes treatment to avoid administration of systemic immunosuppression. Wang *et al*. designed electrospun polymer nanofibers with hydrogel cores that could maintain transplanted syngeneic, allogeneic, or xenogeneic islets and # cells upon transplantation into the peritoneal cavity of mice and dogs. The encapsulated cells showed correction of type 1 diabetes for up to 200 days after implantation in mice. The polymer devices could be retrieved with minimal fibrosis, and cells retained viability. This study supports the potential utility of this nanofibrous device as a feasible approach for improving cell-based treatment for diabetes.

Science Translational Medicine (ISSN 1946-6242) is published by the American Association for the Advancement of Science. 1200 New York Avenue NW, Washington, DC 20005. The title *Science Translational Medicine* is a registered trademark of AAAS.